3

Single-link Flexible Manipulator

3.1 INTRODUCTION

This chapter deals with the investigation to explore the effect of generic payload on the modal parameters, nonlinear behavior, and dynamic performance of single-link flexible manipulator under Cartesian and revolute motions mounted on a planar bidirectional moving platform. Two dynamic models of manipulator with an arbitrarily oriented sizeable payload having inertia whose center of gravity doesn't coincide with the point of attachment have been developed, to determine the modal parameters i.e., natural frequency and corresponding mode-shape. There have been previous literature regarding the modal analysis of single-link manipulator with a payload having mass as well as inertia. However, the studies lacks in demonstrating the effect of other system parameters on the eigenspectrums of single-link manipulator. Therefore, in this chapter the extensive and rigorous study of influence of system parameters and payload attributes has been conducted. In first case, the small deformation model of a rotating planar Cartesian motion at the roller supported end with a pulsating constraint asymmetric force imitating its working environment has been considered, while in second case, the manipulator is assumed to have harmonic revolute joint. These modal parameters are then illustrated graphically upon varying parameters like offset parameters (i.e., offset mass, offset inertia, offset length), mass and stiffness of actuator and hub. Initially, modal analysis has been studied to demonstrate graphically the eigenfrequencies and corresponding eigenspectrums while it is being noted that the system possesses distinct and different vibration characteristics as compared to that of a system without offset payload. A smooth sinusoidal torque as input has been introduced to assess the time dependency factors and parameters which can describes its position inaccuracy over the time.

Further, an investigation into the nonlinear dynamics of the Cartesian manipulator system accounting of geometric nonlinearity and a large deflection model of a flexible rotating manipulator considering both transverse and axial deformation has been carried out. The primary and secondary resonance conditions arising respectively due to transverse harmonic motion and direct forcing conditions in first case while in second case, parametric excitations due to the harmonic motion of the hub have been examined thoroughly. Current research further investigates the influences of offset parameters, mass and stiffness of the actuator, frequency and amplitude of axial force on the steady-state responses for the primary and sub-harmonic resonance conditions to reveal the built-in saddle-node and pitchfork bifurcation due to which the system losses its structural stability. The obtained results have been validated numerically within the permissible error at the assorted critical points in frequency characteristic curves. This work provides an insight into the modal characteristics, and nonlinear behavior of two different models of single-link flexible manipulator with a generic payload. The present results offer specific guidelines towards the designing and control aspects of such manipulators based on the selection of offset parameters.

3.2 MATHEMATICAL MODELING

Fig. 3.1 shows a schematic diagram of a deformed single-link flexible rotating Cartesian manipulator incorporating payload with a general offset where an asymmetric harmonic force $\{F_0 + F_1 cos(\Omega_2 t)\}$ is applied to the paylaod. One end of the link has a roller supported ac-

tuator, while at the other end, an offset payload having mass and inertia is attached. The link is theoretically modeled based on Euler-Bernoulli beam element and the elastic deformation is assumed to be small as compared to the length of the link, i.e., $w(x,t) \ll L$. The manipulator is given a planar general motion $(\vartheta(t), \eta(t))$ through a moving platform at the roller supported end, v_a is the vertical displacement of actuator from the equilibrium position and manipulator is assumed to rotate (Ω) about an axis perpendicular to the plane. The rotation of end point of link can be regarded as $\phi = \tan^{-1}(w'_L) \approx w'_L$.

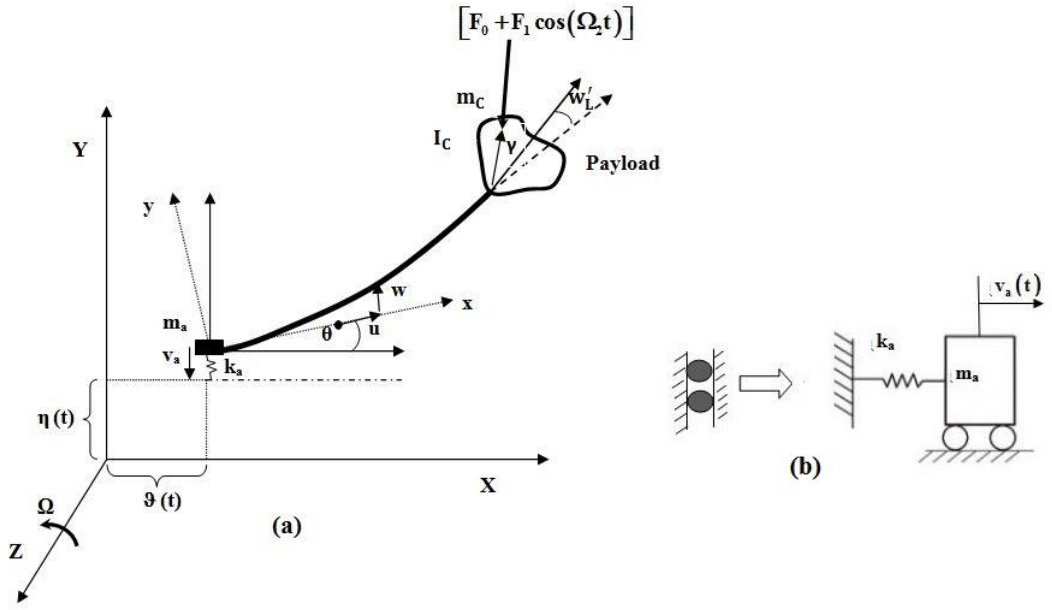

Fig. 3.1: Schematic diagram of (a) rotating Cartesian manipulator with generic payload and (b) flexible actuator.

The position and velocity vectors of a general point on the link and center of gravity of payload are respectively expressed as

$$\vec{q} = (u+x)\hat{x} + (w+y)\hat{y} + \vartheta\hat{X} + (v_a+\eta)\hat{Y},$$
$$\vec{P}_C = \left(u_L + L + c\cos(\gamma + w'_L)\right)\hat{x} + \left(w_L + c\sin(\gamma + w'_L)\right)\hat{y} + \vartheta\hat{X} + (v_a+\eta)\hat{Y}. \quad (3.1)$$

Here, γ is the offset angle, c is the distance of centroid of payload from the point of attachment with the link and θ is the angle of rotation of moving reference frame (x,y) with respect to inertial reference frame (X,Y).

The total energy of the system is composed of kinetic energy (T_{total}) due to the mass of link, actuator and the rotational energy of payload; the potential energy (U_{total}) consists of strain energy due to elastic bending in link, axial stretching and elastic stain in actuator stiffness, are expressed as:

$$T_{total} = m_C \dot{\vec{P}}_C^T \dot{\vec{P}}_C + \int_0^L \rho \dot{\vec{q}}^T \dot{\vec{q}} dx + m_a \left\{ \left(\dot{v}_a + \dot{\eta} + \dot{w}_{(x=0)}\right)^2 + \left(\vartheta + \dot{u}_{(x=0)}\right)^2 \right\} + I_C \left(\dot{w}'_L + \dot{\theta}\right)^2. \quad (3.2)$$

$$U_{total} = (1/2)\left(\int_0^L EI(w'')^2 dx + \int_0^L EA\left(u' + (1/2)w'^2\right)^2 dx + \int_0^L k_a \left(v_a + \eta + w_{(x=0)}\right)^2 dx \right). \quad (3.3)$$

3.3 CARTESIAN SINGLE-LINK FLEXIBLE MANIPULATOR WITH GENERIC PAYLOAD

Using extended Hamilton's principle $\int_{t_1}^{t_2}\left(\delta(T-U)\right)dt=\delta W+\delta W_{nc},\delta(t_1)=\delta(t_2)$; here δW is zero and δW_{nc} is the non-conservative word done by structural damping(c_d) .and Substituting the equations Eqs. (3.1)-(3.3), one may obtain the following governing equations of motion with associated boundary conditions for non-rotating manipulator as:

$$EIw''''+\rho A\begin{pmatrix}\ddot{w}+\ddot{\eta}+\ddot{v}_a+u\ddot{\theta}+x\ddot{\theta}+2\dot{\theta}\dot{u}+\\ \theta\dot{\theta}\dot{\eta}+\theta\dot{v}_a\dot{\theta}-w\dot{\theta}^2-\ddot{\vartheta}\theta\end{pmatrix}+c_d\dot{w}-EA\left(\left(u''+w'w''\right)w'+\left(u'+w'^2/2\right)w''\right)=0. \quad (3.4)$$

$$EIw_L''''-m_c\begin{bmatrix}\ddot{w}_L+\ddot{\eta}+\ddot{v}_a+u_L\ddot{\theta}+L\ddot{\theta}+2\dot{\theta}\dot{u}_L+\theta\dot{\theta}\dot{\eta}+\theta\dot{\theta}\dot{v}_a-w_L\dot{\theta}^2-\\ \ddot{\vartheta}\theta-2c\dot{\theta}\dot{w}_L'\sin\left(\gamma+w_L'\right)-c\dot{\theta}^2\sin\left(\gamma+w_L'\right)+c\ddot{w}_L'\cos\left(\gamma+w_L'\right)\\ -c\dot{w}_L'^2\sin\left(\gamma+w_L'\right)+c\ddot{\theta}\cos\left(\gamma+w_L'\right)\end{bmatrix}-EA\left(u_L'+w_L'^2/2\right)w_L'=0,$$

$$m_C\begin{bmatrix}c^2\ddot{w}_L'+\ddot{w}_Lc\cos\left(\gamma+w_L'\right)+c^2\ddot{\theta}+\ddot{\eta}c\cos\left(\gamma+w_L'\right)+\ddot{v}_ac\cos\left(\gamma+w_L'\right)\\ +cL\ddot{\theta}\cos\left(\gamma+w_L'\right)-\ddot{\vartheta}c\sin\left(\gamma+w_L'\right)-\ddot{\eta}c\theta\sin\left(\gamma+w_L'\right)-\ddot{v}_ac\theta\sin\left(\gamma+w_L'\right)\\ -c\ddot{u}_L\sin\left(\gamma+w_L'\right)+c\dot{\theta}\dot{\eta}\theta\cos\left(\gamma+w_L'\right)+c\dot{\theta}\dot{v}_a\theta\cos\left(\gamma+w_L'\right)-\\ c\dot{\theta}^2w_L\cos\left(\gamma+w_L'\right)-\ddot{\vartheta}c\theta\cos\left(\gamma+w_L'\right)+2c\dot{\theta}\dot{u}_L\cos\left(\gamma+w_L'\right)+\\ c\ddot{\theta}u_L\cos\left(\gamma+w_L'\right)+c\ddot{\theta}w_L\sin\left(\gamma+w_L'\right)-c\theta\dot{\theta}\dot{\vartheta}\sin\left(\gamma+w_L'\right)+\\ 2c\dot{\theta}w_L\sin\left(\gamma+w_L'\right)+cu_L\dot{\theta}^2\sin\left(\gamma+w_L'\right)+c\dot{\theta}^2L\sin\left(\gamma+w_L'\right)\end{bmatrix}-EIw_L''-I_C\ddot{w}'=0,$$

$$EIw_{(0,t)}'''+m_a\left(\ddot{\eta}+\ddot{v}_a+\ddot{w}_{(0,t)}\right)+k_a\left(\eta+v_a+w_{(0,t)}\right)=0,\ EIw_{(0,t)}'=0. \quad (3.5)$$

$$EA\left(u''+w'w''\right)-\rho A\left(\ddot{u}+\ddot{\vartheta}+\theta\ddot{\eta}+\theta\ddot{v}_a-2\dot{w}\dot{\theta}-w\ddot{\theta}-u\dot{\theta}^2+\theta\dot{\theta}\dot{\vartheta}-x\dot{\theta}^2\right)=0. \quad (3.6)$$

$$m_C\begin{pmatrix}\ddot{u}_L+\ddot{\vartheta}+\theta\ddot{\eta}+\theta\ddot{v}_a-w_L\ddot{\theta}-2\dot{w}_L\dot{\theta}+\theta\dot{\theta}\dot{\vartheta}-L\dot{\theta}^2-u_L\dot{\theta}^2-c\ddot{w}_L'\sin\left(\gamma+w_L'\right)\\ -c\dot{w}_L'^2\cos\left(\gamma+w_L'\right)-c\ddot{\theta}\sin\left(\gamma+w_L'\right)-2c\dot{\theta}\dot{w}_L'\cos\left(\gamma+w_L'\right)-c\dot{\theta}^2\cos\left(\gamma+w_L'\right)\end{pmatrix}+EAu_L'=0,$$

$$EA\left(u'+v'^2/2\right)_{(0,t)}-m_a\ddot{\vartheta}=0. \quad (3.7)$$

3.3.1 Modal analysis: free vibration

The equation of motion and boundary conditions can further be reduced to that obtained by [Coleman and McSweeney, 2004], by neglecting the actuator motion and putting the offset equal to zero. Neglecting coupled nonlinear terms and the rotary motion of the motor from Eqs. (3.4)-(3.7), resulting equations of motion and boundary conditions can be used for modal analysis. Deflection functions $r(x,t)$ and $s(x,t)$ are written $r(x,t)=w(x,t)+\eta(t)+v_a(t)$ and $s(x,t)=u(x,t)+\upsilon(t)$. The solutions of *r(x,t)* and *s(x,t)* are explicit functions of space and time, and they can be written as $r(x,t)=U^n(x)T(t)$ and $s(x,t)=W^n(x)T(t)$, where $U^n(x)$, and $W^n(x)$ represent the admissible functions in longitudinal and transverse directions of a Cartesian manipulator and $T(t)$ denotes time modulation. The solution of the resulting equations of motion can be expressed:

$$U^n(x)=R_1^n\cos\left\{\left(\bar{\delta}^2\right)^n\kappa\bar{x}\right\}+R_2^n\sin\left\{\left(\bar{\delta}^2\right)^n\kappa\bar{x}\right\}. \quad (3.8)$$

$$W^n(x)=S_1^n\cos\left(\bar{\delta}^n\bar{x}\right)+S_2^n\cosh\left(\bar{\delta}^n\bar{x}\right)+S_3^n\sin\left(\bar{\delta}^n\bar{x}\right)+S_4^n\sinh\left(\bar{\delta}^n\bar{x}\right). \quad (3.9)$$

The unknowns $(S_1,\cdots S_4,R_1,R_2)^n$ can be evaluated from a set of six algebraic equations derived from the boundary conditions and expressed in the following matrix form with the nondimensional terms: $\delta^2=\omega_m(\rho A/EI)^{1/2}$, $\alpha_{mC}=m_C/\rho AL$, $\alpha_I=I_C/\rho AL^3$, $\alpha_{ma}=m_a/\rho AL$, $\Omega_a=\left((k_a/m_a)/\omega_m^2\right)$, $\kappa^2=I/AL^2$, and $\alpha_c=c/L$.

$$\sum_{i,j=1}^{6}N\left(S^n,R^n,\bar{\delta}^n\right)\Rightarrow\begin{bmatrix}0&0&N_{13}&N_{14}&0&0\\N_{21}&N_{22}&N_{23}&N_{24}&0&0\\N_{31}&N_{32}&N_{33}&N_{34}&N_{35}&N_{36}\\N_{41}&N_{42}&N_{43}&N_{44}&0&0\\0&0&0&0&N_{55}&N_{56}\\N_{61}&N_{62}&N_{63}&N_{64}&N_{65}&N_{66}\end{bmatrix}\begin{Bmatrix}S_1^n\\S_2^n\\S_3^n\\S_4^n\\R_1^n\\R_2^n\end{Bmatrix}=\begin{bmatrix}0\\0\\0\\0\\0\\0\end{bmatrix}. \tag{3.11}$$

The elements of the matrix followed are illustrated as:

$$N_{13}=1,N_{14}=1,N_{21}=N_{22}=\alpha_{ma}\bar{\delta}^n\left(\Omega_a{}^2-1\right),N_{23}=-1,N_{24}=1,$$

$$N_{31}=-\cos\left(\bar{\delta}^n\right)-\alpha_{mC}\left(\bar{\delta}^n\right)^2\left(-\alpha_C{}^2\bar{\delta}^n\sin\left(\bar{\delta}^n\right)+\alpha_C\cos(\gamma)\cos\left(\bar{\delta}^n\right)\right)+\alpha_I\left(\bar{\delta}^n\right)^3\sin\left(\bar{\delta}^n\right),$$

$$N_{32}=\cosh\left(\bar{\delta}^n\right)-\alpha_{mC}\left(\bar{\delta}^n\right)^2\left(\alpha_C{}^2\bar{\delta}^n\sinh\left(\bar{\delta}^n\right)+\alpha_C\cos(\gamma)\cosh\left(\bar{\delta}^n\right)\right)-\alpha_I\left(\bar{\delta}^n\right)^3\sinh\left(\bar{\delta}^n\right),$$

$$N_{33}=-\sin\left(\bar{\delta}^n\right)-\alpha_{mC}\left(\bar{\delta}^n\right)^2\left(\alpha_C{}^2\bar{\delta}^n\cos\left(\bar{\delta}^n\right)+\alpha_C\cos(\gamma)\sin\left(\bar{\delta}^n\right)\right)-\alpha_I\left(\bar{\delta}^n\right)^3\cos\left(\bar{\delta}^n\right),$$

$$N_{34}=\sinh\left(\bar{\delta}^n\right)-\alpha_{mC}\left(\bar{\delta}^n\right)^2\left(\alpha_C{}^2\bar{\delta}^n\cosh\left(\bar{\delta}^n\right)+\alpha_C\cos(\gamma)\sinh\left(\bar{\delta}^n\right)\right)-\alpha_I\left(\bar{\delta}^n\right)^3\cosh\left(\bar{\delta}^n\right),$$

$$N_{35}=\alpha_{mc}\alpha_c\sin(\gamma)\left(\bar{\delta}^n\right)^2\cos\left(\kappa\left(\bar{\delta}^n\right)^2\right),\ N_{36}=\alpha_{mc}\alpha_c\sin(\gamma)\left(\bar{\delta}^n\right)^2\sin(\gamma)\sin\left(\kappa\left(\bar{\delta}^n\right)^2\right),$$

$$N_{36}=\alpha_{mc}\alpha_c\sin(\gamma)\left(\bar{\delta}^n\right)^2\sin(\gamma)\sin\left(\kappa\left(\bar{\delta}^n\right)^2\right),$$

$$N_{41}=\sin\left(\bar{\delta}^n\right)+\alpha_{mC}\bar{\delta}^n\left(\cos\left(\bar{\delta}^n\right)-\bar{\delta}^n\alpha_C\cos(\gamma)\sin\left(\bar{\delta}^n\right)\right),$$

$$N_{42}=\sinh\left(\bar{\delta}^n\right)+\alpha_{mC}\bar{\delta}^n\left(\cosh\left(\bar{\delta}^n\right)+\bar{\delta}^n\alpha_C\cos(\gamma)\sinh\left(\bar{\delta}^n\right)\right),$$

$$N_{43}=-\cos\left(\bar{\delta}^n\right)+\alpha_{mC}\bar{\delta}^n\left(\sin\left(\bar{\delta}^n\right)+\bar{\delta}^n\alpha_C\cos(\gamma)\cos\left(\bar{\delta}^n\right)\right),$$

$$N_{44}=\cosh\left(\bar{\delta}^n\right)+\alpha_{mC}\bar{\delta}^n\left(\sinh\left(\bar{\delta}^n\right)+\bar{\delta}^n\alpha_C\cos(\gamma)\cosh\left(\bar{\delta}^n\right)\right),$$

$$N_{55}=\alpha_{ma}\kappa\left(\bar{\delta}^n\right)^2,\ N_{56}=1,\ N_{61}=-\alpha_{mC}\alpha_C\left(\bar{\delta}^n\right)^3\kappa\sin(\gamma)\sin\left(\bar{\delta}^n\right),$$

$$N_{62}=\alpha_{mC}\alpha_C\left(\bar{\delta}^n\right)^3\kappa\sin(\gamma)\sinh\left(\bar{\delta}^n\right),\ N_{62}=\alpha_{mC}\alpha_C\left(\bar{\delta}^n\right)^3\kappa\sin(\gamma)\sinh\left(\bar{\delta}^n\right),$$

$$N_{63}=\alpha_{mC}\alpha_C\left(\bar{\delta}^n\right)^3\kappa\sin(\gamma)\cos\left(\bar{\delta}^n\right),\ N_{64}=\alpha_{mC}\alpha_C\left(\bar{\delta}^n\right)^3\kappa\sin(\gamma)\cosh\left(\bar{\delta}^n\right),$$

$$N_{65}=-\sin\left(\kappa\left(\bar{\delta}^n\right)^2\right)-\alpha_{mC}\left(\bar{\delta}^n\right)^2\kappa\cos\left(\kappa\left(\bar{\delta}^n\right)^2\right),\ N_{66}=\cos\left(\kappa\left(\bar{\delta}^n\right)^2\right)-\alpha_{mC}\left(\bar{\delta}^n\right)^2\kappa\sin\left(\kappa\left(\bar{\delta}^n\right)^2\right). \tag{3.12}$$

The condition for a non-trivial solution yields in a characteristic frequency equation which can be solved numerically to obtain the eigenfrequencies of respective modes of vibration. Therefore, determinant of coefficient of matrix of Eq. (3.11) leads to a transcendental polynomial equation of $\bar{\delta}$ in the form of design parameters.

$$det\left|N\left(S^n,R^n,\bar{\delta}^n\right)\right|=0. \tag{3.13}$$

Here $N\left(S^n, R^n, \bar{\delta}^n\right)$ represent the coefficient matrix. For a given set of values of various system parameters defined above, the roots of the Eq. (3.13) provide the frequency parameters $\left(\bar{\delta}\right)$ which can be further used to depict the corresponding mode shapes. In terms of unit magnitude of S_1, the expressions of $S_2 \cdots S_4, R_{1,2}$ are given below:

$$\pi_1 = -\frac{N_{21}}{N_{22}},\ \pi_2 = \frac{N_{14}N_{23} - N_{13}N_{24}}{N_{22}N_{13}},\ \pi_3 = \frac{-N_{31}N_{55}N_{13} - \pi_1 N_{32}N_{13}N_{55}}{N_{36}N_{13}N_{55} - N_{35}N_{56}N_{13}},$$

$$\pi_4 = \frac{N_{33}N_{55}N_{14} - \pi_2 N_{32}N_{55}N_{13} - N_{34}N_{13}N_{55}}{N_{36}N_{13}N_{55} - N_{35}N_{56}N_{13}},$$

$$S_4 = \frac{-N_{13}\left(N_{61}N_{55} + \pi_1 N_{62}N_{55} - \pi_3 N_{65}N_{56} + \pi_3 N_{66}N_{55}\right)}{\pi_2 N_{62}N_{13}N_{55} - N_{14}N_{63}N_{55} + N_{64}N_{13}N_{55} - \pi_4 N_{65}N_{56}N_{13} + \pi_4 N_{66}N_{13}N_{55}},\quad S_2 = \pi_1 + \pi_2 S_4,$$

$$S_3 = \frac{-N_{14}S_4}{N_{13}},\quad R_2 = \pi_3 + \pi_4 S_4,\ \text{and}\ R_1 = \frac{-N_{56}R_2}{N_{55}}. \tag{3.14}$$

3.3.2 Nonlinear forced vibration analysis

In this sub-section, the effect of parameters associated with general payload and linear actuator on the dynamic responses under asymmetric pulsating tip force and harmonic base motion are highlighted. The source of nonlinearity is mainly due to the link flexibility accounting of geometric stretching effect. From the available literature, it is established that the effect of mass of payload on the nonlinear dynamics of the manipulator with geometric/inertial nonlinearities have been studied significantly. Hence, here we additionally explore theThe inherent role of offset payload well as actuator parameters onto the structural stability. An appropriate motion has further been imparted at the roller-supported end as base motion. A complex and complete equation of motion is expressed as below:

$$EIw'''' + \rho A\left(\ddot{w} + \ddot{\eta} - \Omega^2 w\right) - EA\left\{\left(3/2\right)w'^2 w''\right\} + c_d\dot{w} - m_C\Omega^2\left\{L + c\cos\left(\gamma\right)\right\}w'' -$$
$$\rho A\Omega^2\left\{\left(L^2 - x^2\right)w'\right\}' - \left\{F_0 + F_1\cos\left(\Omega_2\right)\right\}\cos\left(\gamma\right)w'' - \left\{F_0 + F_1\cos\left(\Omega_2\right)\right\}\sin\left(\gamma\right) = 0. \tag{3.15}$$

Henceforth, $(')$ and $(\cdot)$ represent the differentiation with respect to the nondimensional space $\bar{x}$ and time τ, respectively. The first mode of any vibratory system is found to be most vulnerable one as most of the excitation energy is being injected into the first mode of vibration when the system is being excited with a broadband signal.

To discretize the governing equation of motion Eq. (3.15), one may use the following assumed mode expression:

$$\bar{q}\left(\bar{x}, \tau\right) = r\varphi\left(\bar{x}\right)p\left(\tau\right). \tag{3.16}$$

Here, $p\left(\tau\right)$ is the time modulation, scaling factor is represented by r in above equation and $\varphi(\bar{x})$ is the eigenfunction of cantilevered link with offset-payload expressed as:

$$\varphi\left(\bar{x}\right) = S_1\cos\left(\bar{\delta}\bar{x}\right) + S_2\cosh\left(\bar{\delta}\bar{x}\right) + S_3\sin\left(\bar{\delta}\bar{x}\right) + S_4\sinh\left(\bar{\delta}\bar{x}\right). \tag{3.17}$$

Here, $\bar{\delta}$ is the absolute value of the smallest possible root of the transcendental equation Eq. (3.13) & the constants, $S_1 \ldots S_4$, can be calculated as explained in previous section. The harmonic Cartesianp motion of manipulator is expressed as. $\bar{\eta} = \eta_0\left(x\right)\cos\left(\Omega_1\tau\right)$. Now Eq. (3.15) is withwritten in terms of dimensionless variables: $\bar{\mathrm{w}} = \mathrm{w}/r$, $\bar{x} = x/L$, $\bar{c} = \left(c_d L^2/\sqrt{\rho AEI}\right)$, $\tau = t\left(EI/\rho AL^4\right)$, $\bar{\Omega} = \Omega\sqrt{\rho AL^4/EI}$, $r = \sqrt{I/A}$, $\bar{F}_0 = \left(\pi^2 F_0/4F_c\right)$, $\bar{F}_1 = \left(F_1 L^2/EI\right)$. Here, F_c is the critical buckling load of the link, and using Eq. (3.16) along with the orthogonal property of

the mode shapes and dropping the bar for the sake of simplicity, the following dimensionless equation of motion can be found.

$$\ddot{p}(\tau)+\omega^2 p(\tau)+\bar{c}\dot{p}(\tau)-\bar{\alpha}_1\Omega_1^2\cos(\Omega_1\tau)-\bar{\alpha}_4\sin(\gamma)\cos(\Omega_2\tau)-\bar{\alpha}_2 p^3(\tau)-\bar{\alpha}_3 p(\tau)\cos(\gamma)\cos(\Omega_2\tau)=0. \tag{3.18}$$

Here,

$$\omega^2=\left[\begin{array}{l}\left(\int_0^1\varphi''''(\bar{x})\varphi(\bar{x})d\bar{x}\Big/\int_0^1\varphi^2(\bar{x})d\bar{x}\right)-\Omega^2\left\{\int_0^1\left(1-\bar{x}^2\right)\varphi''(\bar{x})\varphi(\bar{x})d\bar{x}\Big/\int_0^1\varphi^2(\bar{x})d\bar{x}\right\}\\ \quad-\left\{\bar{F}_0+\alpha_{mC}\Omega^2\left(1+\alpha_c\cos(\gamma)\right)\right\}\left(\int_0^1\varphi''(\bar{x})\varphi(\bar{x})d\bar{x}\Big/\int_0^1\varphi^2(\bar{x})d\bar{x}\right)-\Omega^2\end{array}\right],$$

$$\alpha_1=(\eta_0)\left(\int_0^1\varphi(\bar{x})d\bar{x}\Big/\int_0^1\varphi^2(\bar{x})d\bar{x}\right),\ \alpha_2=(3/2)\left(\int_0^1\varphi'^2(\bar{x})\varphi''(\bar{x})\varphi(\bar{x})d\bar{x}\Big/\int_0^1\varphi^2(\bar{x})d\bar{x}\right),$$

$$\alpha_3=\bar{F}_1\left(\int_0^1\varphi(\bar{x})\varphi''(\bar{x})d\bar{x}\Big/\int_0^1\varphi^2(\bar{x})d\bar{x}\right),\ \text{and}\ \alpha_4=\bar{\bar{F}}_1\left(\int_0^1\varphi(\bar{x})\varphi''(\bar{x})d\bar{x}\Big/\int_0^1\varphi^2(\bar{x})d\bar{x}\right). \tag{3.19}$$

The frequency ω in Eq. (3.19) is not the actual frequency but instead a normalized one. Now, a small dimensionless parameter, ε is introduced to order the terms in Eq. (3.18) and the resulting equation is expressed as:

$$\ddot{p}(\tau)+\omega^2 p(\tau)+\varepsilon\left\{2\xi\dot{p}(\tau)-\alpha_3 p(\tau)\cos(\gamma)\cos(\Omega_2\tau)\right\}-\varepsilon^2\left\{\begin{array}{l}\alpha_1\Omega_1^2\cos(\Omega_1\tau)+\alpha_2 p^2(\tau)+\\ \alpha_4\sin(\gamma)\cos(\Omega_2\tau)\end{array}\right\} \tag{3.20}$$

Here, $\bar{\alpha}_1=\varepsilon^2\alpha_1,\bar{\alpha}_2=\varepsilon^2\alpha_2,\bar{\alpha}_3=\varepsilon\alpha_3,\bar{\alpha}_4=\varepsilon^2\alpha_4$, and $\bar{c}=2\varepsilon\xi$. Since the nondimensional temporal equation contains many nonlinear terms, the approximate solution of the above equation is carried out using method of multiple scales as one of the perturbation method. The displacement is expressed in term of various times scales such as T_0,T_1,T_2 and can be written in the following form:

$$p=p_1(T_0,T_1,T_2)+\varepsilon p_2(T_0,T_1,T_2)+\varepsilon^2 p_3(T_0,T_1,T_2). \tag{3.21}$$

Here, $T_0=\tau,T_1=\varepsilon\tau,$ and $T_2=\varepsilon^2\tau$ are different time scales and hence, p is determined as a function of these time scales instead of τ. Using chain rule, time derivatives in terms of $T_0,T_1,$ and T_2 become;

$$d/d\tau=\partial/\partial T_0+\varepsilon\partial/\partial T_1+\varepsilon^2\partial/\partial T_2,\text{and}$$

$$d^2/d\tau^2=\partial^2/\partial T_0{}^2+2\varepsilon\left(\partial^2/\partial T_0\partial T_1\right)+\varepsilon^2\left(2\left(\partial^2/\partial T_0\partial T_2\right)+\partial^2/\partial T_1{}^2\right). \tag{3.22}$$

Substituting Eqs. (3.21)-(3.22) into Eq. (3.20) and equating the coefficients of the same powers of ε and yields the following equations:

$$O\left(\varepsilon^0\right):\ \partial^2 p_1/\partial T_0{}^2+\omega^2 p_1=0. \tag{3.23}$$

$$\mathrm{O}\left(\varepsilon^1\right):\partial^2 p_2/\partial T_0{}^2+2\left(\partial^2 p_1/\partial T_0\partial T_1\right)+\omega^2 p_2-\alpha_3 p_1\cos(\gamma)\cos(\Omega_2\tau)+2\xi\left(\partial p_1/\partial T_0\right)=0. \tag{3.24}$$

$$\mathrm{O}\left(\varepsilon^2\right):\ \begin{array}{l}\partial^2 p_3/\partial T_0{}^2+\omega^2 p_3+2\left(\partial^2 p_2/\partial T_0\partial T_1\right)+\partial^2 p_1/\partial T_1{}^2+2\left(\partial^2 p_1/\partial T_0\partial T_2\right)-\\ \alpha_2 p_1{}^3+2\xi\left(\partial p_1/\partial T_1+\partial p_2/\partial T_2\right)-\alpha_1\Omega_1{}^2\cos(\Omega_1 T_0)-\alpha_4\sin(\gamma)\cos(\Omega_2 T_0)=0.\end{array} \tag{3.35}$$

The general solution of Eq. (3.23) can be expressed as:

$$p_1 = A(T_1,T_2)\exp(i\omega T_0) + \bar{A}(T_1,T_2)\exp(-i\omega T_0). \tag{3.26}$$

Here, $\bar{A}(\mathrm{T}_1,\mathrm{T}_2)$ is the complex conjugate of $A(T_1,T_2)$. Putting Eq. (3.26) into Eq. (3.24) gives:

$$\begin{aligned}\partial^2 p_2 / \partial \mathrm{T}_0{}^2 + \omega^2 p_2 = &-2\mathrm{i}\omega(\partial A/\partial \mathrm{T}_1)\exp(\mathrm{i}\omega \mathrm{T}_0) - 2\mathrm{i}\xi\omega A\exp(\mathrm{i}\omega \mathrm{T}_0) + \\ &\alpha_3\left\{A\mathrm{e}(\mathrm{i}(\omega+\Omega_2)\mathrm{T}_0) + \bar{A}\exp(\mathrm{i}(\Omega_2-\omega)\mathrm{T}_0)\right\}\cos(\gamma) + cc.\end{aligned} \tag{3.27}$$

Here, cc stands for the complex conjugate.

3.3.3 Case I: subharmonic resonance $(\Omega_2 \approx 2\omega)$

Using similar procedures as explained in [Hamed et al., 2018] & [Pratiher and Dwivedy, 2011], and substituting $\Omega_2 = 2\omega + \varepsilon\sigma_1$ into Eq. (3.25), and eliminating the terms proportional to $\exp(i\omega T_0)$ and $\exp(-i\omega T_0)$, that leads to the secular terms, one may obtain the following equation:

$$2i\omega(\partial A/\partial T_1) = -2i\mu\omega A + \left(\alpha_2 \bar{A}\cos(\gamma)/2\right)\exp(i\sigma_1 T_1). \tag{3.28}$$

Therefore, the particular solution of Eq. (3.25) yields:

$$p_2 = \left[\alpha_2 A\cos(\gamma)/2\left\{\omega^2 - \left(\omega^2 + \Omega_2{}^2\right)\right\}\right]\exp(i(\omega+\Omega_2)). \tag{3.29}$$

Similarly, for the response p_3, the following expression is obtained:

$$\begin{aligned}&\partial^2 p_3/\partial \mathrm{T}_0{}^2 + \omega^2 p_3 = \left(\alpha_1 \Omega_1{}^2/2\right)\exp(i\Omega_1 T_0) + \alpha_2 A^3\exp(3\mathrm{i}\omega \mathrm{T}_0) + \\ &\left\{-2\mathrm{i}\omega(\partial A/\partial \mathrm{T}_2) + \partial^2 A/\partial \mathrm{T}_1{}^2 + 3\alpha_1 A^2\bar{\mathrm{A}} - 2\xi(\partial A/\partial T_1)\right\}\exp(\mathrm{i}\omega \mathrm{T}_0) \\ &+\left\{\alpha_3 A(\omega+\Omega_2)\cos(\gamma)/2\left[\omega^2 - \left(\omega^2+\Omega_2{}^2\right)\right]\right\}\exp\{(\omega+\Omega_2)T_0\} + \mathrm{cc}.\end{aligned} \tag{3.30}$$

On elimination of the secular terms, one may obtain the following expression:

$$2i\bar{\Omega}(\partial A/\partial T_2) = \xi^2 A - \left[\alpha_3{}^2 A\{cos(\gamma)\}^2/16\omega^2\right] - \left(\alpha_3\sigma_1 A/4\bar{\Omega}\right)\exp(i\sigma_1 T_1) + 3\alpha_2 A^2\bar{A}. \tag{3.31}$$

Now, expressing the governing equation in terms of original time variable τ by substituting Eq. (3.28) and Eq. (3.31) in $dA/d\tau = \partial A/\partial T_0 + \varepsilon\partial A/\partial T_1 + \varepsilon^2\partial A/\partial T_2$, one can obtain:

$$\begin{aligned}&-2i\bar{\Omega}(\partial A/\partial\tau) + \left\{\varepsilon^2\xi^2 - 2i\mu\varepsilon\omega - \varepsilon^2\alpha_3{}^2\{\cos(\gamma)\}^2/16\omega^2\right\}A + \\ &\bar{A}\left\{\left(\varepsilon\alpha_3\cos(\gamma)/2\right) - \left(\varepsilon^2\alpha_3\sigma_1\cos(\gamma)/4\bar{\Omega}\right)\right\}\exp(i\sigma_1 T_1) + 3\alpha_2\varepsilon^2 A^2\bar{A} = 0.\end{aligned} \tag{3.32}$$

Now, $\mathrm{A}(\tau)$ is expressed in polar form equal to $(1/2)\mathrm{a}_1(\tau)\mathrm{e}^{\mathrm{i}\lambda_1(\tau)}$, where $\mathrm{a}_1(\tau)$ and $\lambda_1(\tau)$ are the amplitudes and phase angle of the response. With substitution of $A(\tau)$ into Eq. (3.32) and separating real and imaginary parts, one may obtain the following autonomous equations as below.

$$\begin{aligned}&-\omega(\partial a_1/\partial\tau) - \varepsilon\omega\xi a_1 + \left(\varepsilon\alpha_3 cos(\gamma)/4 - \varepsilon^2\alpha_3\sigma_1 cos(\gamma)/8\omega\right)a_1\sin(\varphi_1) = 0,\ \ 2\varphi_1 = \sigma_1 T_1 - 2\lambda_1, \\ &a_1\omega(\partial\varphi_1/\partial\tau) = \left[\begin{array}{l}\varepsilon\omega a_1\sigma_1/2 + 3\varepsilon^2\alpha_2 a_1{}^3/8 + \left\{\xi^2\varepsilon^2 - \alpha_3{}^2\varepsilon^2\left(\cos(\gamma)\right)^2/16\omega^2\right\}a_1/2 + \\ \left(\varepsilon\alpha_3\cos(\gamma)/4 - \varepsilon^2\alpha_3\sigma_1\cos(\gamma)/8\omega\right)a_1\cos(\varphi_1)\end{array}\right].\end{aligned} \tag{3.33}$$

Eq. (3.33) describes the modulation of the amplitude and phase of the free oscillation term. The first order solution in terms of original time variable τ can be expressed as

$$p = (1/2)a_1\cos(\Omega_2\tau - \varphi_2)/2 + \left[\varepsilon\alpha_2 a_1\cos(\gamma)/4\left\{\omega^2 - \left(\omega^2+\Omega_2{}^2\right)\right\}\right]\cos(3\Omega_2 - \varphi_2)/2 + O(\varepsilon).$$

For obtaining steady-state response, $\partial a_1 / \partial \tau$ and $\partial \varphi_1 / \partial \tau$ are set to zero. By eliminating φ_1 from the resultant equations yieldrenders a frequency response equation in terms of a_1 and σ_1. The stability of the steady-state solutions (a_{10}, φ_{10}) is determined by superposing a perturbation (a_{11}, φ_{11}) on the fixed points as $a_1 = a_{10} + a_{11}$, $\varphi_1 = \varphi_{10} + \varphi_{11}$ and investigating the eigenvalues of the Jacobian of the resultant linearized equations.

$$\{\dot{X}\} = \begin{bmatrix} -\varepsilon\xi + Q_1 \sin(\varphi_{10}) / \omega & Q_1 a_{10} \cos(\varphi_{10}) / \omega \\ \varepsilon\sigma / a_0 + 9\varepsilon^2 a_0 / 8\omega + Q_2 / \omega a_0 + Q_1 \cos(\varphi_{10}) / \omega a_0 & -Q_1 \sin(\varphi_{10}) / \omega \end{bmatrix} \{X\} = [J]\{X\}$$

Here,

$$Q_1 = \left(\varepsilon\alpha_3 \cos(\gamma) / 4 - \varepsilon^2 \alpha_3 \sigma_1 \cos(\gamma) / 8\omega\right), \text{ and } Q_2 = \left\{\xi^2\varepsilon^2 / 2 - {\alpha_3}^2 \varepsilon^2 \left(\cos(\gamma)\right)^2 / 32\omega^2\right\}. \quad (3.34)$$

The elements of the Jacobian *[J]* are functions of equilibrium points (a_{10}, φ_{10}) which satisfy the steady-state equations. It may be noted that the steady-state solutions of Eq. (3.33) are stable only if the real part of the eigenvalues of Jacobian matrix *[J]*are negative.

3.3.4 Case II: combined resonance $(\Omega_2 \approx 2\omega, \Omega_1 \approx \omega)$

Considering similar procedures explained in the previous sub-section, one may obtain the following autonomous equations.

$$-\omega(\partial a_2 / \partial \tau) - \varepsilon\omega\xi a_2 + \left(\varepsilon\alpha_3 \cos(\gamma) / 4 - \varepsilon^2 \alpha_3 \sigma_2 \cos(\gamma) / 8\omega\right) a_2 \sin(2\varphi_2 + \xi) + \left(\alpha_1 {\Omega_1}^2 / 2\right) \sin(\varphi_2) = 0,$$

$$a_2 \omega(\partial \varphi_2 / \partial \tau) = \begin{bmatrix} \varepsilon\omega a_2 \sigma + 3\varepsilon^2 \alpha_2 {a_2}^3 / 8 + \left\{\xi^2\varepsilon^2 - {\alpha_3}^2 \varepsilon^2 \left(\cos(\gamma)\right)^2 / 16\omega^2\right\} a_2 / 2 + \\ \left(\varepsilon\alpha_3 \cos(\gamma) / 4 - \varepsilon^2 \alpha_3 \sigma_1 \cos(\gamma) / 8\omega\right) a_2 \cos(\varphi_2 + \xi) + 0.5\alpha_1 \varepsilon^2 {\Omega_1}^2 \cos(\varphi_2) \end{bmatrix}. \quad (3.35)$$

Here, $\varphi_2 = \sigma_2 T_1 - \lambda_2$. The stability of the steady-state solutions of Eq. (3.35) can be determined by understanding the nature of eigenvalues of Jacobian matrix [*J*] following a similar procedure as explained in section 3.1.3. If all the eigenvalues are found to be negative, the steady-state solutions are stable.

3.3.5 Numerical results and discussion

a) *Modal analysis: eigenspectrums*

First, the effect of decision variables on the determination of eigenfrequencies and associated eigenfunctions have been critically studied and graphically demonstrated. First five eigenfrequencies with actuator mass (α_{ma}) has been computed and shown in Table 3-1 while other parameters are kept constant. Eigenfrequency without actuator mass α_{ma} has been computed and compared with the others. The comparison has further been made with the eigenfrequencies calculated by considering zero actuator mass. It is noticed that the eigenfrequency decreases as the actuator mass parameter increases. Adding actuator mass to that ofwith the flexible link, increases the overall inertia of the moving components gets increased and as a result, the eigenfrequency is found to be decreased.

In next section of table, the 1st column $(\Omega_a = 0)$ represents the rigid actuator condition and has been calculated by [Coleman and McSweeney, 2004] for the rollerR-free (R-F) beam condition and similarly, other parameters in the reference can be evaluated by actuator mass variation keeping Ω_a and offset *(c)* equal to zero. The increase in actuator frequency parame-

ter (Ω_a), indicates the increase in stiffness of the actuator. It is evident from the table that the eigenfrequencies increase with the addition of stiffness to the system. Hence, the eigenfrequency varies with the condition of actuator whether it is rigid or flexible.

Table 3-1 : Variation of eigenfrequencies with system parameters

The variation of eigenfrequencies with actuator mass parameter			
$\alpha_{ma}=0$	$\Omega_a=0.5$, $\gamma=0$, $\alpha_I=0.5$, $\alpha_c=0.5$, $\alpha_{mC}=0.5$		
	$\alpha_{ma}=0.5$	$\alpha_{ma}=1.0$	$\alpha_{ma}=5.0$
1.0717	1.0505	1.0372	1.0030
2.9493	2.6548	2.5337	2.3262
5.8357	5.3959	5.2830	5.1434
8.8772	8.3422	8.2453	8.1413
11.9644	11.3751	11.2938	11.2131
The variation of eigenfrequencies with joint frequency parameter			
	$\alpha_{ma}=0.5$, $\alpha_{mC}=0.5$, $\alpha_I=0.5$, $\alpha_c=0.5$, $\gamma=0$		
$\Omega_a=0.0$	$\Omega_a=0.5$	$\Omega_a=1.0$	$\Omega_a=2.0$
2.3650	1.0505	1.0718	1.1636
5.4978	2.6548	2.9493	4.6519
8.6393	5.3959	5.8357	7.8669
11.7809	8.3422	8.8772	11.0246
14.9225	11.3751	11.9644	14.1684
The variation of eigenfrequencies with offset mass and offset moment of inertia parameters			
$\alpha_c=0.0$, $\alpha_{ma}=1.0$, $\Omega_a=0.5$, $\gamma=0$			
α_{mC}			
0.1	0.5	1.0	5.0
α_I =0.1			
1.5872	1.4669	1.3924	1.2567
2.8399	2.7479	2.7082	2.6572
5.5223	5.2547	5.1593	5.0503
8.4970	8.2038	8.1216	8.0386
11.5388	11.2577	11.1906	11.1272
α_I =0.5			
1.1603	1.1345	1.1144	1.0668
2.6182	2.4052	2.2947	2.1265
5.4893	5.2038	5.1019	4.9856
8.4872	8.1900	8.1069	8.0232
11.5346	11.2523	11.1850	11.1214
α_I =1.0			
0.9877	0.9763	0.9669	0.9436
2.5890	2.3540	2.2276	2.0257
5.4852	5.1975	5.0949	4.9777
8.4859	8.1883	8.1051	8.0213
11.5341	11.2516	11.1843	11.1206
The variation of nondimensional eigenfrequencies with offset ratio					
$\alpha_{mC}=0.5$, $\alpha_{ma}=0.5$, $\Omega_a=0.5$, $\gamma=0$					
α_c					
α_I =0.0			α_I =0.5		
0	0.25	0.5	0.0	0.25	0.5
1.7394	1.4981	1.3152	1.1427	1.1008	1.0504
4.4625	3.71372	3.3810	2.5315	2.5942	2.6548

7.4444	6.3882	6.1239	5.3183	5.3499	5.3958
10.4968	9.2827	9.0843	8.2878	8.3074	8.3421
13.5828	12.2802	12.1250	11.3340	11.3477	11.3750

The computation of eigenfrequencies with respect to payload mass (α_{mC}) and inertia (α_I) are also shown where the payload mass and inertia parameters are varied from {0.1 to 5}, and {0.1 to 1}, respectively. It is noteworthy that, as the payload mass increases(α_{mC}), the eigenfrequencies decrease. Similarly, with increase in payload inertia(α_I), the decrease in eigenfrequencies is observed. This is due to fact that with increase in payload mass or inertia, overall effective inertia gets increased which in turn decreases the eigenfrequencies. In last section, the effect of offset length (α_c) on eigenfrequencies with and without payload inertia has been demonstrated. Without payload inertia(α_I), all the eigenfrequencies decrease with offset length(α_c). With payload inertia(α_I), lower eigenfrequencies are found to be decreasing while higher eigenfrequencies tend to increase with increase in offset length. The first column of this section represents the point payload condition. The eigenfrequencies tend to decrease with offset length if the payload inertia parameter is considered as zero. However, as soon as the payload inertia is included in the system, only the lower eigenfrequencies tend to decrease and higher eigenfrequencies tend to increase with offset parameter. It is owing to the fact that the inertia parameter has a tremendous effect on the higher eigenfrequencies and hence the fundamental mode should be controlled in order to achieve more accurate positioning of a heavy payload.

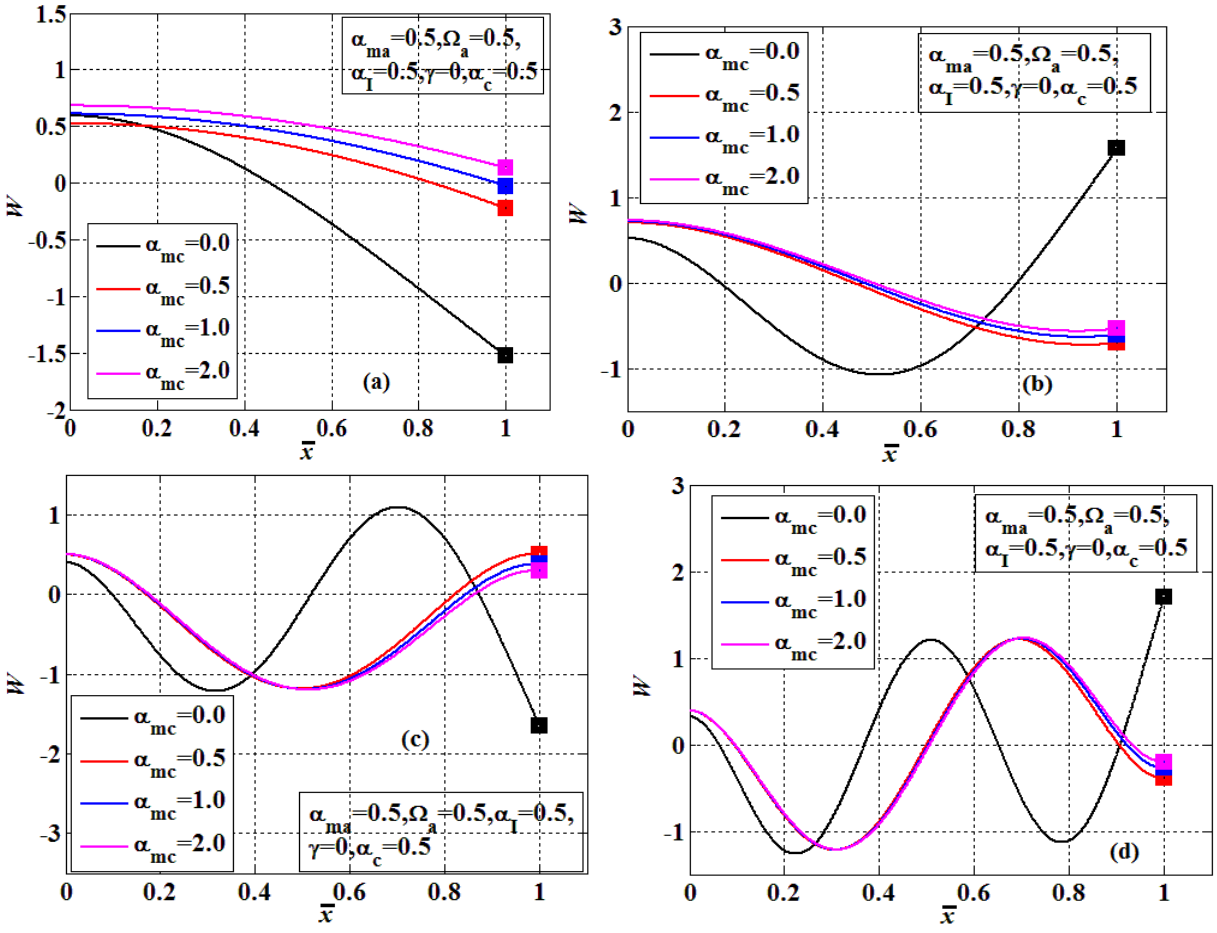

Fig. 3.2: Variation of first four mode shapes of Cartesian manipulator with payload mass (α_{mC}) (a) mode 1 (b) mode 2 (c) mode 3 (d) mode 4.

The normalized eigenfunctions corresponding to the eigenfrequencies have been plotted showing the influence of the offset payload mass (α_{mC}) in Fig. 3.2. The comparison has been made with the zero payload condition $(\alpha_{mC}=0)$. With increase in payload mass (α_{mC}), the mode shapes tend to spread out along its length while a little effect on the amplitude is found at the roller supported end. The shifting of node points towards the payload end is noticed as the payload mass parameter (α_{mC}) is increased.

The effect of actuator mass (α_{ma}) and payload inertia (α_I) on the system mode shapes is seen through the Fig. 3.3. With increase in actuator mass, displacement at the roller-supported end decreases while at the payload end, amplitude tends to clutter together. It has been observed that for higher modes of vibration, the link tends to behave like a beam clamped at the roller supported end. It is also evident that, there is negligible effect of payload inertia on the lower modes of vibration. However, for higher modes of vibration, the increase in payload inertia increases the amplitude of the manipulatorshifts the node towards the free end of the manipulator.

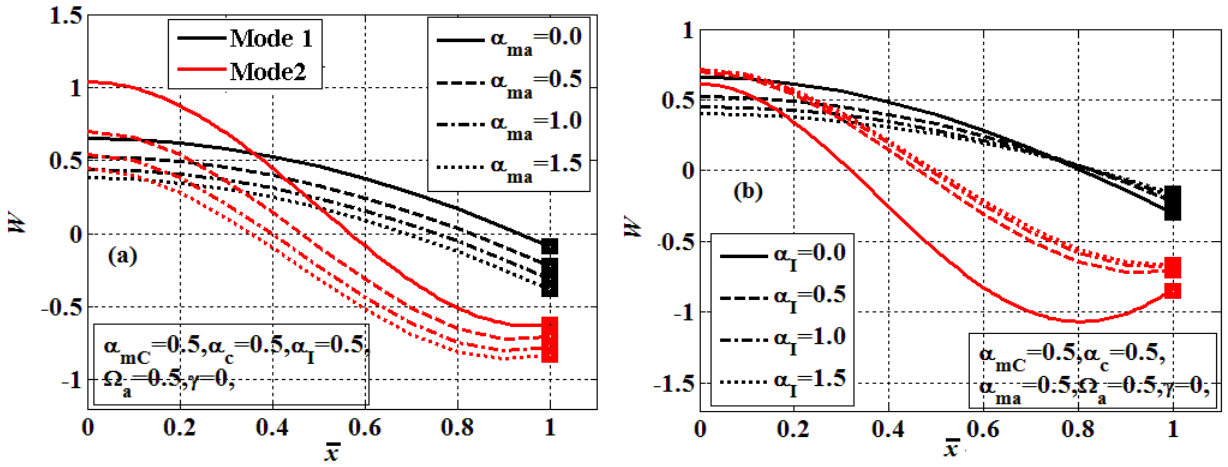

Fig. 3.3: Variation of mode shapes of Cartesian manipulator with (a) actuator mass (α_{ma}) and (b) payload inertia (α_I).

An actuator frequency parameter (Ω_a) equal to zero represents the case when the actuator is assumed to be rigid. The mode shapes corresponding to the non-zero value of Ω_a is compared with it in Fig. 3.4. As The amplitude increases as the actuator frequency parameter (Ω_a) increases until unit magnitude $(\Omega_a=1.0)$, i.e., when the actuator mass–spring frequency equals the system frequency and hence, the actuator dynamics gets decoupled from the manipulator the node shifts to the payload end. If the frequency parameter (Ω_a) increases further, actuator end experiences a large deflectionthe amplitude suddenly.

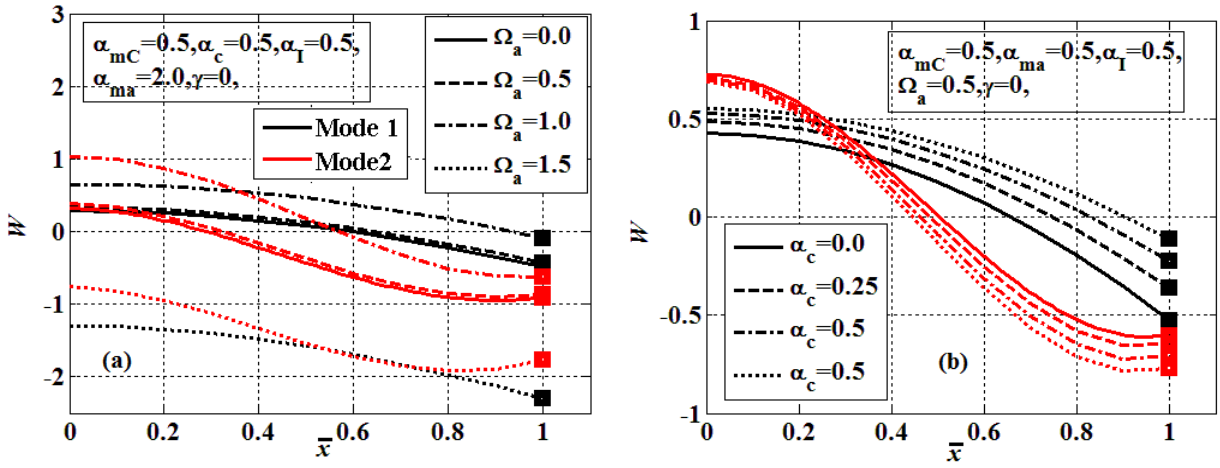

Fig. 3.4: Variation of mode shapes of Cartesian manipulator with (a) actuator frequency parameter (Ω_a) and (b) offset ratio α_c.

The influence of offset ratio (α_c), i.e., ratio between the offset length and the length of the link on the eigenfunctions has also been shown in Fig. 3.4. The manipulator deflection decreases as tends to decrease as the offset ratio increases for the lower vibration modes. However, for the higher modes of vibration the node shifts towards the actuator end as the payload offset is increased. The influence of axial motion on the mode shapes of the manipulator has been shown in Fig. 3.5 . The effect of axial motion is observed to be significant on the mode shapes when the large mass parameter is considered on either ends of the link.

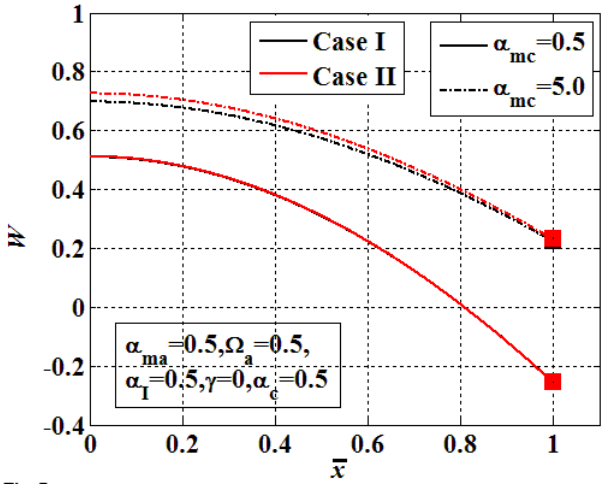

Fig. 3.5: Influence of axial motion on the mode shapes of Cartesian manipulator.

b) *Nonlinear analysis: bifurcation and stability*

In previous section, the influence of various system parameters on the eigenfrequencies and subsequent eigenfunctions prior to the investigation of the dynamic behavior of the flexible manipulator is demonstrated. The computation of modal parameters always guides the design engineer to select the appropriate operating conditions in order to avoid resonance condition that causes the unwanted excessive vibration and noise. The system here undergoes primary resonance condition when the frequency of the harmonic base motion becomes nearly equal to the system' normalized natural frequency. In addition, the manipulator experiences subharmonic resonance condition when the frequency of the pulsating constraint axial force becomes nearly double of the manipulator frequency. A pictorial representation has been developed to study the effect of offset parameters onto the system dynamics and associated vibrations. For this simulation, the beam element with length L= 0.35 m0.3m, width b = 0.3 m, thickness h

=0.003 m, mass-density ρ = 7800 kg/m^3, Young's modulus E=2E =.1x1011 N/m2210 GPa, damping parameter (ξ) as 0.01, amplitude ratio (η_0) as 0.05, small dimensionless parameter ε as 0.1, force parameters $\bar{F}_0$ and $\bar{F}_1$ as 0.001 have been considered. Fig. 3.6 depicts a frequency response curves for the subharmonic (I) and combined resonance (II) cases showing the vibration amplitudes with forcing frequency. In all the figures solid and dashed lines represent stable and unstable solutions, respectively. In both the cases, due to the presence of nonlinearities, multiples solutions are observed resulting in jump phenomenon. Here multiple solutions are observed with an existence of pitchfork bifurcation for sub-harmonic resonance case while saddle-node bifurcation for combined resonance case. For sub-harmonic condition, the system experiences the sudden jump phenomena at sub-critical pitchfork bifurcation (G). For the frequencies beyond point G, the system exhibits multiple solutions where the actual response is decided by the initial conditions. Below the super-critical pitchfork bifurcation (D), the system always vibrates with negligible amplitude. The system only undergoes trivial responses when it is operated at points A and F, while at other points, manipulator experiences both trivial and nontrivial responses.

In the unstable region (D-G), i.e., sub-critical and super-critical pitchfork bifurcation, the manipulator vibrates with amplitude lying on the upper branch of frequency response curve since the trivial solution is found to be unstable. In the second case of combined resonance, both jump down and jump up phenomena have been observed respectively from J or M, based on the condition of sweeping up and down from the respective starting points. The amplitude of the system between the unstable region, i.e., between J and M shall be decided by initial conditions. Hence, repeated occurrence of this jump phenomenon may often lead to fatigue failure for the present system or similar ones.

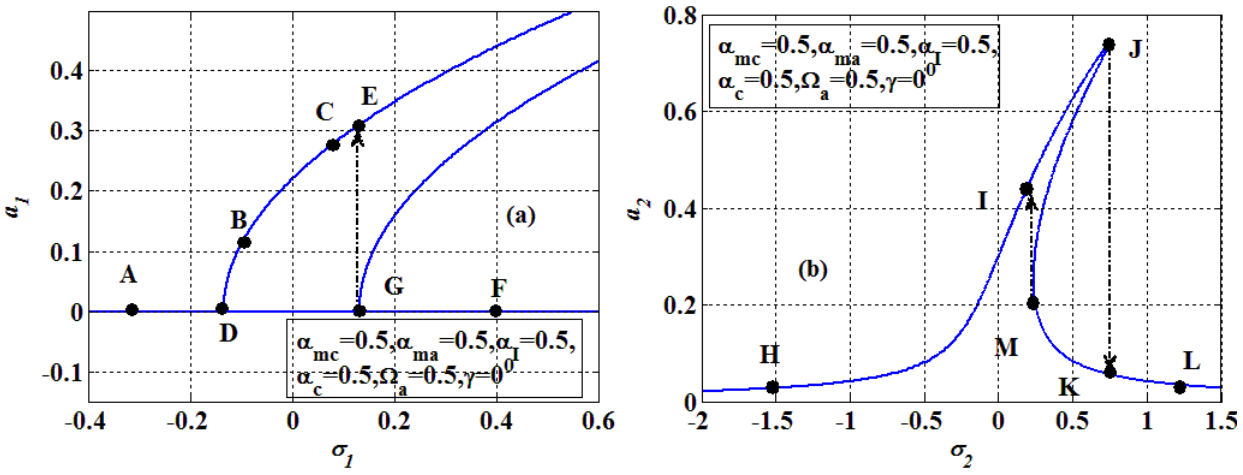

Fig. 3.6: Frequency response characteristics of Cartesian manipulator (a) Subharmonic resonance (b) Combined primary-subharmonic resonance.

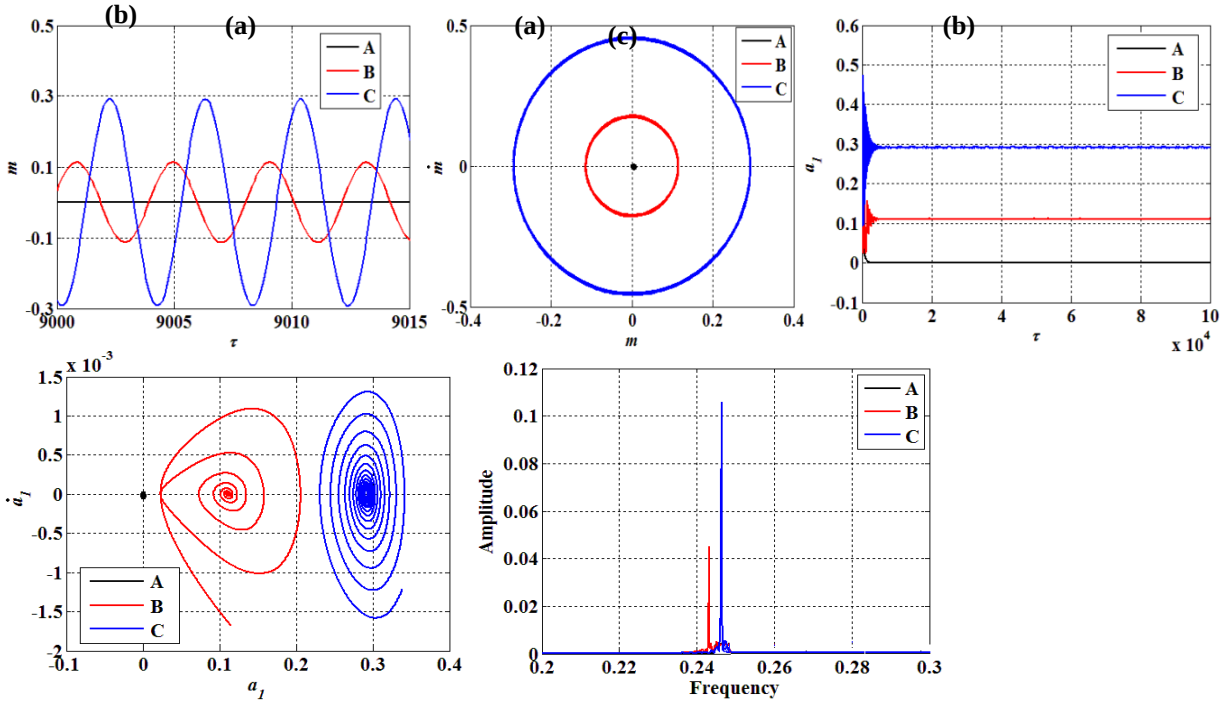

Fig. 3.7: Analytical (a) numerical (b) time response and phase portrait , FFT (c) of critical points A, B, and C identified in Fig. 3.6.

Numerical simulation to compute time responses, phase portraits, and Fourier spectrum at critical points are carried out by numerically solving Eq. (3.18) and are compared with the findings depicted in Fig. 3.7 using method of multiple scales. These results are found to be in good agreement.

For the no payload condition, the effect of offset payload (α_{mC}) on the frequency response curves has been demonstrated in Fig. 3.8. The behavior of the manipulator is observed to suddenly shift from spring softening to hardening with the payload mass in both cases up to 0.5. With further increase in payload mass from 0.5 to 1.5, the amplitude starts increasing for a specific forcing frequency. The unstable region of sub-harmonic case also suddenly increases with increase in payload mass.

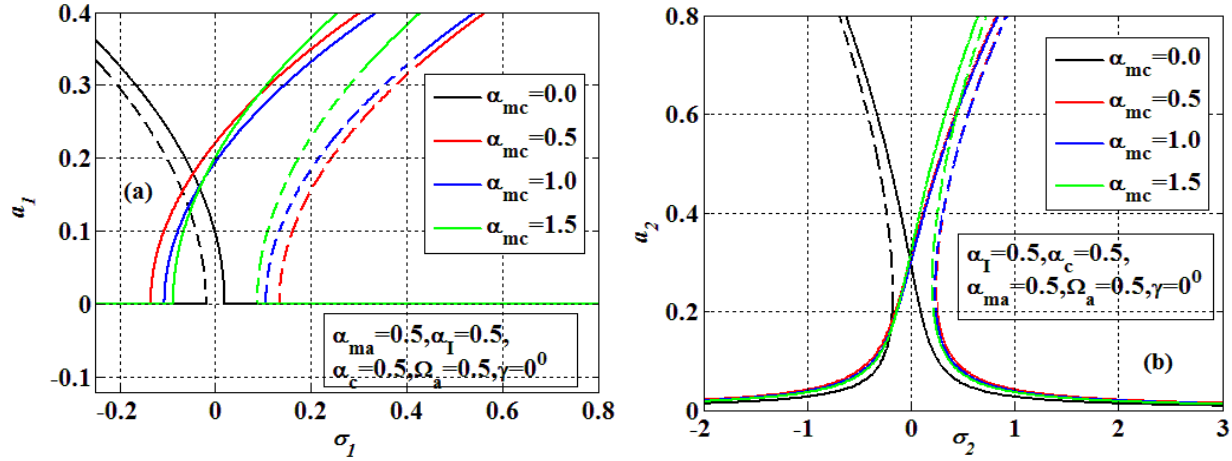

Fig. 3.8: Effect of payload mass parameter (α_{mc}) on the frequency response curves (a) Subharmonic resonance (b) Combined primary-subharmonic resonance.

The behavior of nonlinear responses has been noticed to shift from spring hardening to softening with the actuator mass parameter (α_{ma}) in both the resonance cases as shown in Fig. 3.9. For a small actuator mass (α_{ma}), the maximum amplitude increases for a specific excitation frequency with a negligible change in unstable regions. Influences of payload inertia (α_I) on frequency response curves have been shown in Fig. 3.10. It is evident that the amplitude of vibration increases with payload inertia for a fixed forcing frequency. Actuator frequency parameter (Ω_a) represents the stiffness of actuator and has been varied to investigate its significance on dynamic behavior as depicted in Fig. 3.11. The vibration amplitude decreases significantly with increase in stiffness of the actuator and also affecting the unstable region in both the cases.

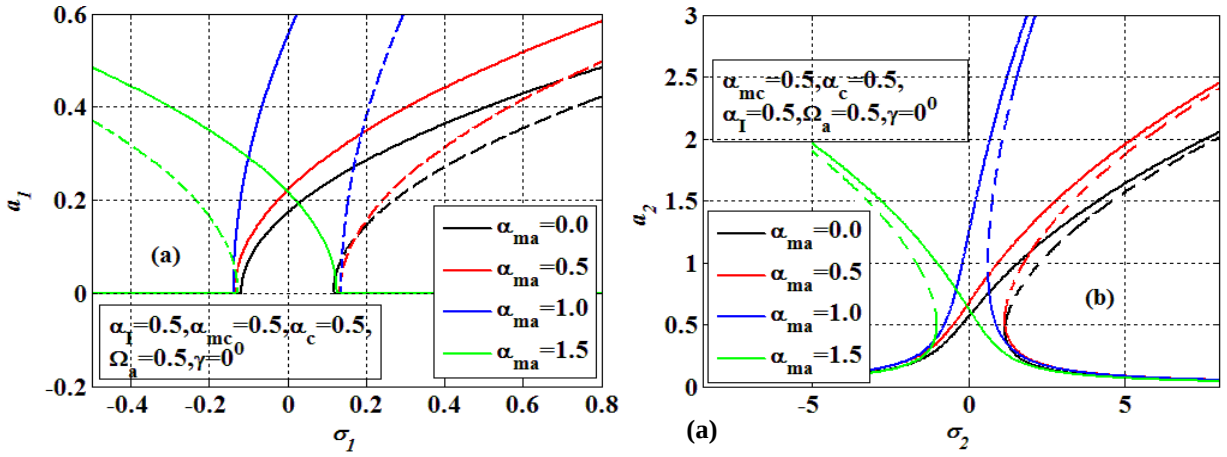

Fig. 3.9: Effect of actuator mass parameter (α_{ma}) on the frequency response curves (a) Subharmonic resonance (b) Combined primary-subharmonic resonance.

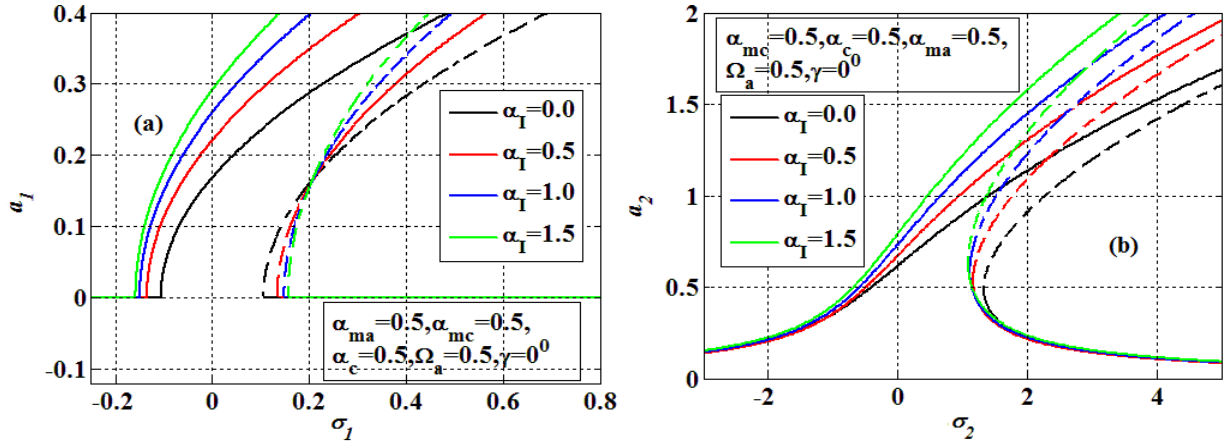

Fig. 3.10: Effect of payload inertia parameter (α_I) on the frequency response curves (a) Subharmonic resonance (b) Combined primary-subharmonic resonance.

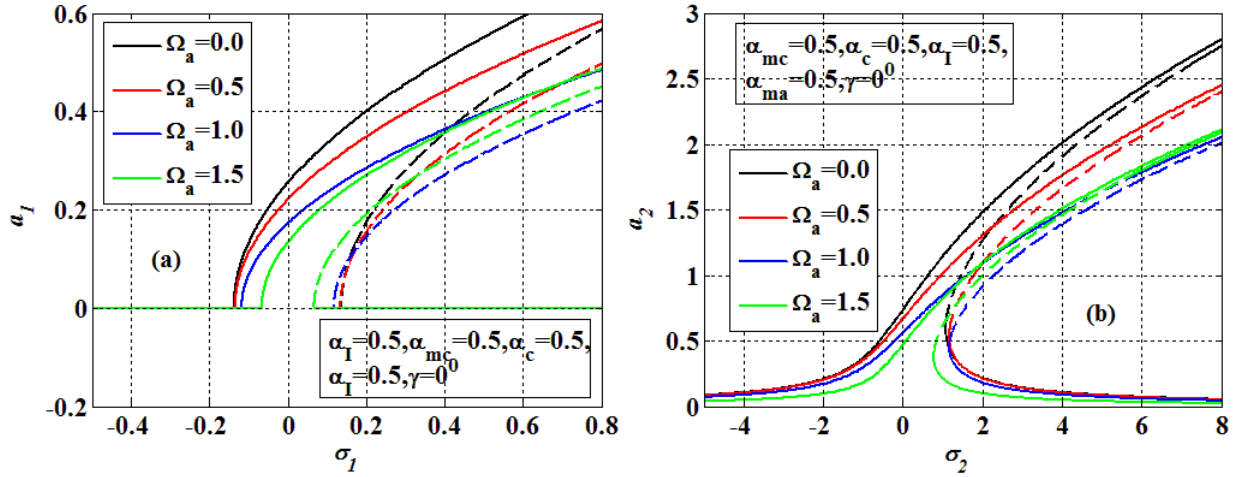

Fig. 3.11: Effect of actuator frequency parameter (Ω_a) on the frequency response curves (a) Subharmonic resonance (b) Combined primary-subharmonic resonance.

It is observed in Fig. 3.12, the system exhibits a typical softening behavior for point payload $(\alpha_c = 0)$. It is noteworthy that the behavior changes to spring hardening from the spring softening when the center of gravity of the payload is moved further away from the point of attachment. Amplitude of vibration is found to be decreased with increase in offset ratio (α_c) for a specific forcing frequency.

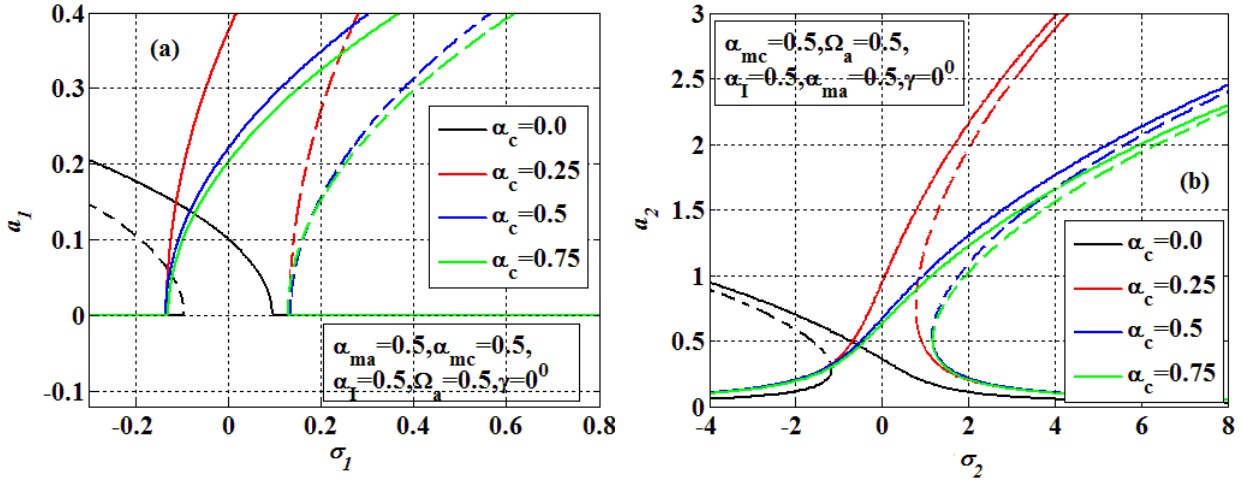

Fig. 3.12: Effect of offset ratio (α_c) on the frequency response curves (a) Subharmonic resonance (b) Combined primary-subharmonic resonance.

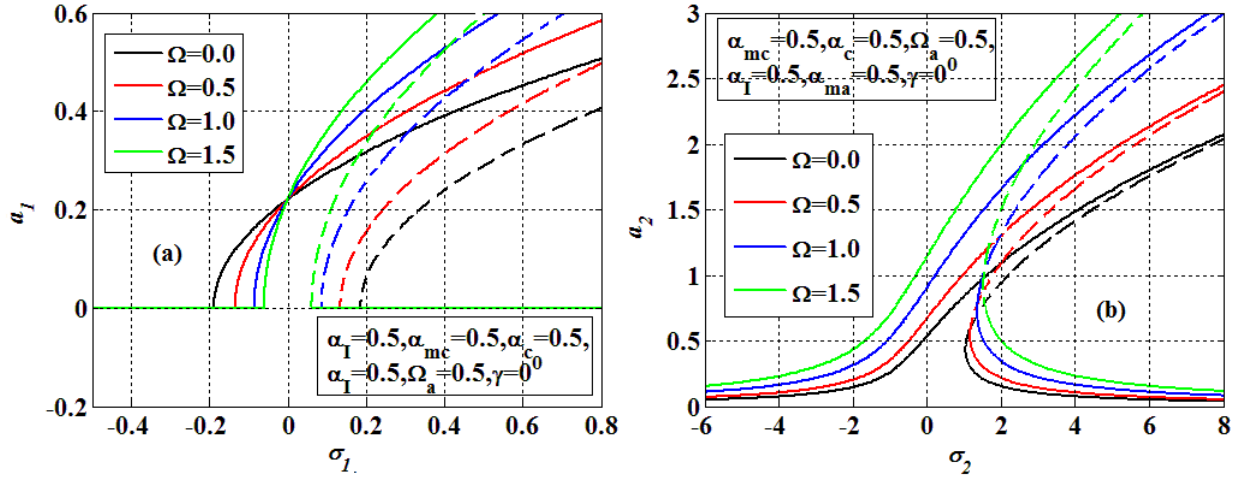

Fig. 3.13: Effect of rotating frequency (Ω) on the frequency response curves (a) Subharmonic resonance (b) Combined primary-subharmonic resonance.

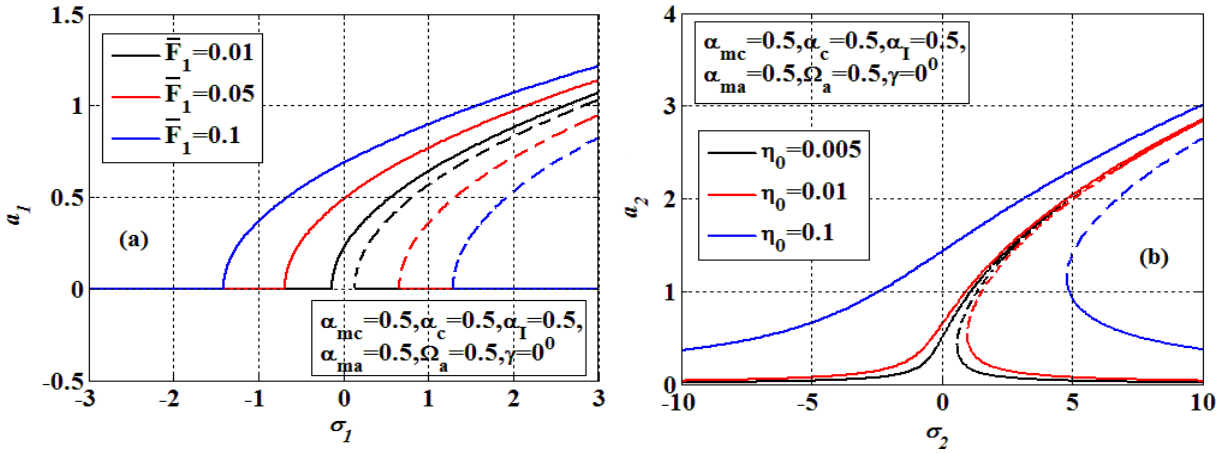

Fig. 3.14: Effect of amplitude of axial force and base motion on the frequency response curves (a) Subharmonic resonance (b) Combined primary-subharmonic resonance.

It is noticed in Fig. 3.13 that the jump length and unstable region of the system has been started increasing with the increase in rotating frequency (Ω) resulting in the increase of maximum amplitude of the system. The influence of the amplitude of harmonic force $(\bar{F}_1)$ and base motion (η_0) on the respective frequency response curves for subharmonic and combined resonance condition is described in Fig. 3.14. In both the cases, the unstable regions and vibration amplitudes increase significantly with the forcing amplitudes.

3.4 SINGLE-LINK FLEXIBLE MANIPULATOR WITH REVOLUTE HUB

A deflected configuration of a flexible robotic manipulator modeled as Euler-Bernoulli beam with revolute hub incorporating a generic offset payload mounted on a moving platform $\{\vartheta(t), \eta(t)\}$ is shown in Fig. 3.15. The manipulator is subjected to a harmonic revolute motion at the hub end and generic payload has been attached at the distal end. The hub is modeled as a linear spring-inertia system. In this section, the large deformation model of the flexible single-link manipulator with rotary joint is considered. Further, eigenespectrums are calculated to further facilitate the nonlinear analysis of the manipulator with harmonic revolute joint motion to investigate the influence of payload and hub parameters.

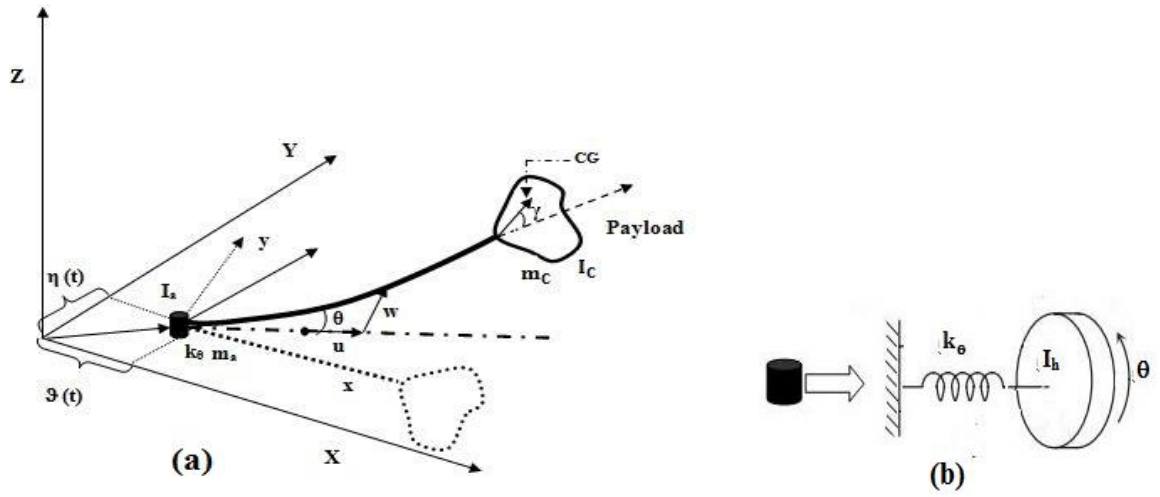

Fig. 3.15: Schematic diagram of (a) flexible manipulator with (b) revolute hub incorporating a generic payload mounted on moving base.

The kinetic energy (T_{total}) of the overall system due to inertia of the link, payload, actuator, and joint is expressed as:

$$T_{Total} = (1/2)\left\{ m_C \vec{P}_C^T \vec{P}_C + m_h \left(\left(\dot{\eta} + \dot{w}_{(x=0)} \right)^2 + \left(\vartheta + \dot{u}_{(x=0)} \right)^2 \right) + \int_0^L \rho \vec{\dot{q}}^T \vec{\dot{q}} dx + I_C \left(\dot{w}'_L + \dot{\theta} \right)^2 + I_h \dot{\theta}^2 \right\}. \quad (3.36)$$

Similarly, the total potential energy of the manipulator (U_{total}) is composed of the elastic bending for large deformation, axial deformation, and torsional spring deformation are given as:

$$U_{Total} = (1/2)\left\{ \int_0^L EI \left(w'' \right)^2 \left(1 + w'^2 \right)^2 dx + \int_0^L EA \left(u' \right)^2 + \int_0^L k_\theta \theta^2 dx \right\}. \quad (3.37)$$

The rotation speed (Ω) is neglected from Eq. (3.33) to obtain the general point and center of gravity of payload.

3.4.1 Governing equations

Substituting Eqs. (3.36)-(3.37) into $\int_{t_1}^{t_2} \left(\delta \left(T - U \right) \right) dt = \delta W + \delta W_{nc}, \delta \left(t_1 \right) = \delta \left(t_2 \right)$; here $W \left(= \bar{\tau} \theta \right)$ is the work done by torque applied at the joint and δW_{nc} is the non-conservative word done by structural damping (c_d), to further derive the equations of motions and corresponding boundary conditions in axial and transverse directions along with rotational motion of the hub as:

$$EI\left\{ w'''' + \left(w' \left(w' w'' \right)' \right) \right\} + c_d \dot{w} + \rho A \left(\ddot{w} + \ddot{\eta} + u\ddot{\theta} + x\ddot{\theta} + 2\dot{\theta}\dot{u} + \theta\dot{\theta}\dot{\eta} - w\dot{\theta}^2 - \ddot{\vartheta}\theta \right) = 0. \quad (3.38)$$

$$EIw'''_L - m_c \begin{Bmatrix} \ddot{w}_L + \ddot{\eta} + u_L\ddot{\theta} + L\ddot{\theta} + 2\dot{\theta}\dot{u}_L + \theta\dot{\theta}\dot{\eta} - w_L\dot{\theta}^2 - \ddot{\vartheta}\theta - c\dot{w}_L'^2 \sin(\gamma) \\ + c\ddot{\theta}\cos(\gamma) - 2c\dot{\theta}\dot{w}'_L \sin(\gamma_L) - c\dot{\theta}^2 \sin(\gamma) + c\ddot{w}'_L \cos(\gamma) \end{Bmatrix} = 0,$$

$$m_C \{ c^2 \ddot{w}'_L + \ddot{w}_L c\cos(\gamma) + c^2\ddot{\theta} + \ddot{\eta}c\cos(\gamma_L) + cL\ddot{\theta}\cos(\gamma) - \ddot{\vartheta}c\sin(\gamma) - \ddot{\eta}c\theta\sin(\gamma) -$$

$$c\ddot{u}_L \sin(\gamma) + c\dot{\theta}\dot{\eta}\theta\cos(\gamma) - c\dot{\theta}^2 w_L \cos(\gamma) + 2c\dot{\theta}\dot{u}_L \cos(\gamma) + c\ddot{\theta}u_L \cos(\gamma) -$$

$$c\theta\dot{\theta}\dot{\vartheta}\sin(\gamma) - c\dot{\theta}w'_L \sin(\gamma) + cu_L\dot{\theta}^2 \sin(\gamma) + c\dot{\theta}^2 L\sin(\gamma) + c\ddot{\theta}w_L \sin(\gamma) - \ddot{\vartheta}c\theta\cos(\gamma)\}$$

$$+EIw''_L + I_C \left(\ddot{w}'_L + \ddot{\theta} \right) = 0,$$

$$EIw'''_{(0,t)} + m_h \left\{ \ddot{\eta} + \ddot{w}_{(0,t)} \right\} = 0, \; EIw'_{(0,t)} = 0. \quad (3.39)$$

$$EAu'' - \rho A \left(\ddot{u} + \ddot{\vartheta} + \theta\ddot{\eta} - w\ddot{\theta} - 2\dot{w}\dot{\theta} + \theta\dot{\theta}\dot{\vartheta} - x\dot{\theta}^2 - u\dot{\theta}^2 \right) = 0. \quad (3.40)$$

$$m_C \begin{Bmatrix} \ddot{u}_L + \ddot{\vartheta} + \theta\ddot{\eta} - w_L\ddot{\theta} - 2\dot{w}_L\dot{\theta} + \theta\dot{\theta}\dot{\vartheta} - L\dot{\theta}^2 - u_L\dot{\theta}^2 - c\dot{\theta}^2\cos(\gamma) - \\ c\ddot{w}'_L \sin(\gamma) - c\dot{w}'^2_L \cos(\gamma) - c\ddot{\theta}\sin(\gamma) - 2c\dot{\theta}\dot{w}'_L \cos(\gamma) \end{Bmatrix} + EAu'_L = 0,$$

$$EA\{u'\}_{(0,t)} - m_h \left\{ \ddot{\vartheta} + \ddot{u}_{(0,t)} \right\} = 0. \quad (3.41)$$

$$I_h\ddot{\theta}+k_\theta\theta+I_C\left(\ddot{\theta}+\ddot{w}_L'\right)-\int_0^L\rho A\begin{Bmatrix}x\theta\ddot{\vartheta}+w\ddot{u}+w\ddot{\vartheta}-w^2\ddot{\theta}-u\ddot{\eta}-u\ddot{w}-u^2\ddot{\theta}-\\ x\ddot{w}-x\ddot{\eta}-x^2\ddot{\theta}-2w\dot{\theta}\dot{w}+w\theta\ddot{\eta}-2u\dot{\theta}\dot{u}-\\ 2x\dot{\theta}\dot{u}+u\theta\ddot{\vartheta}-2xu\ddot{\theta}+\dot{\eta}^2\theta+\theta\dot{\eta}\dot{w}+\dot{\vartheta}^2\theta+\dot{u}\theta\dot{\vartheta}\end{Bmatrix}-$$

$$m_C\begin{Bmatrix}c\ddot{\vartheta}\sin(\gamma)+L\theta\ddot{\vartheta}-c\ddot{\eta}\cos(\gamma)+2L\dot{\theta}\dot{w}_L'\sin(\gamma)+c\theta\ddot{\eta}\sin(\gamma)+cL\dot{w}_L'^2\sin(\gamma)-\\ cL\ddot{w}_L'\cos(\gamma)-2Lc\ddot{\theta}\cos(\gamma)-L\ddot{\eta}-c^2\ddot{\theta}+c\theta\ddot{\vartheta}\cos(\gamma)-c\ddot{w}_L'\cos(\gamma)-\\ 2c\dot{\theta}\dot{w}_L\sin(\gamma)-cw_L\ddot{w}_L'\sin(\gamma)-cw_L\dot{w}_L'^2\cos(\gamma)-2cw_L\ddot{\theta}\sin(\gamma)\\ +w_L\ddot{u}_L+w_L\ddot{\vartheta}-w^2{}_L\ddot{\theta}-u_L\ddot{\eta}-u_L\ddot{w}_L-u^2{}_L\ddot{\theta}-L\ddot{w}_L-2c\dot{\theta}\dot{u}_L\cos(\gamma)\\ +w_L\theta\ddot{\eta}-L^2\ddot{\theta}+cu_L\dot{w}_L'^2\sin(\gamma)-cu_L\ddot{w}_L'\cos(\gamma)-2cu_L\ddot{\theta}\cos(\gamma)-\\ c^2w_L'+2cu_L\dot{w}_L\dot{\theta}\sin(\gamma)-2cw_L\dot{w}_L'\dot{\theta}\cos(\gamma)-2w_L\dot{\theta}\dot{w}_L+c\ddot{u}_L\sin(\gamma)\\ -2u_L\dot{\theta}\dot{u}_L-2L\dot{\theta}\dot{u}_L+u_L\theta\ddot{\vartheta}-2Lu_L\ddot{\theta}+\dot{\eta}^2\theta+\theta\dot{\eta}\dot{w}_L+c\theta\dot{\eta}\dot{w}_L'\cos(\gamma)\\ +\dot{\vartheta}^2\theta+\dot{u}_L\theta\dot{\vartheta}+c\theta\dot{\vartheta}\dot{w}_L'\sin(\gamma)\end{Bmatrix}=\bar{\tau}. \tag{3.42}$$

The derived equations of motion and boundary conditions represent a flexible mobile robotic manipulator consisting of a flexible link, flexible rotating hub, a generic payload, moving platform and geometric nonlinearity. In the modal analysis, the coupled nonlinear and damping terms from Eqs. (3.38)-(3.42) are neglected. It can be observed that the linear boundary conditions in transverse and axial direction are coupled if the offset becomes non-axial to the axis of manipulator. Now, the transverse and longitudinal deflections of the manipulator in terms of a new function in space and time are established as, $r(x,t)$ and $s(x,t)$ as $r(x,t)=w(x,t)+\eta(t)+x\theta$ and $s(x,t)=u(x,t)+\vartheta(t)$, respectively. Here $w(x,t)$, $u(x,t)$, and θ represent transverse, longitudinal, and joint motion, respectively imparted as harmonic function of system frequency.

$$s(x,t)=U^n(x)\cos(\omega_m t),\ r(x,t)=W^n(x)\cos(\omega_m t),\ \theta(t)=\theta_0\cos(\omega_m t). \tag{3.43}$$

Here, $U^n(x)$ and $W^n(x)$ represent the longitudinal and transverse eigenfunction, respectively, θ_0 as angular rotational amplitude and ω_m is unknown eigenfrequency of the whole system. By substituting Eqs. (3.43) into equations of motion in longitudinal and transverse directions; after solving the equation, the nth longitudinal and transverse mode shapes of the manipulator similar to those given in Eq. (3.10) are obtained. Six algebraic equations in terms of integration constants $(S_1....S_4,R_1,R_2)^n$ by following the procedure explained in section 3.1.1 are obtained and the resulting equations are expressed in matrix form whose coefficients are given as:

$$N_{11}=\sin\left(\bar{\delta}^n\right)+\alpha_{mC}\bar{\delta}^n\left(\cos\left(\bar{\delta}^n\right)-\bar{\delta}^n\alpha_c\cos(\gamma)\sin\left(\bar{\delta}^n\right)\right),$$

$$N_{12}=\sinh\left(\bar{\delta}^n\right)+\alpha_{mC}\bar{\delta}^n\left(\cosh\left(\bar{\delta}^n\right)+\bar{\delta}^n\alpha_c\cos(\gamma)\sinh\left(\bar{\delta}^n\right)\right),$$

$$N_{13}=-\cos\left(\bar{\delta}^n\right)+\alpha_{mC}\bar{\delta}^n\left(\sin\left(\bar{\delta}^n\right)+\bar{\delta}^n\alpha_c\cos(\gamma)\cos\left(\bar{\delta}^n\right)\right),$$

$$N_{14}=\cosh\left(\bar{\delta}^n\right)+\alpha_{mC}\bar{\delta}^n\left(\sinh\left(\bar{\delta}^n\right)+\bar{\delta}^n\alpha_c\cos(\gamma)\cosh\left(\bar{\delta}^n\right)\right),$$

$$N_{21}=-\cos\left(\bar{\delta}^n\right)-\alpha_{mC}\left(\bar{\delta}^n\right)^2\left(-\alpha_c^2\bar{\delta}^n\sin\left(\bar{\delta}^n\right)+\alpha_c\cos(\gamma)\cos\left(\bar{\delta}^n\right)\right)+\alpha_I\left(\bar{\delta}^n\right)^3\sin\left(\bar{\delta}^n\right),$$

$$N_{22}=\cosh\left(\bar{\delta}^n\right)-\alpha_{mC}\left(\bar{\delta}^n\right)^2\left(\alpha_c{}^2\bar{\delta}^n\sinh\left(\bar{\delta}^n\right)+\alpha_c\cos(\gamma)\cosh\left(\bar{\delta}^n\right)\right)-\alpha_I\left(\bar{\delta}^n\right)^3\sinh\left(\bar{\delta}^n\right),$$

$$N_{23}=-\sin\left(\bar{\delta}^n\right)-\alpha_{mC}\left(\bar{\delta}^n\right)^2\left(\alpha_c{}^2\bar{\delta}^n\cos\left(\bar{\delta}^n\right)+\alpha_c\cos(\gamma)\sin\left(\bar{\delta}^n\right)\right)-\alpha_I\left(\bar{\delta}^n\right)^3\cos\left(\bar{\delta}^n\right),$$

$$N_{24}=\sinh\left(\bar{\delta}^n\right)-\alpha_{mC}\left(\bar{\delta}^n\right)^2\left(\alpha_c{}^2\bar{\delta}^n\cosh\left(\bar{\delta}^n\right)+\alpha_c\cos(\gamma)\sinh\left(\bar{\delta}^n\right)\right)-\alpha_I\left(\bar{\delta}^n\right)^3\cosh\left(\bar{\delta}^n\right),$$

$$N_{25}=\alpha_{mC}\alpha_c\left(\bar{\delta}^n\right)^2\sin(\gamma)\cos\left(\kappa\left(\bar{\delta}^n\right)^2\right),N_{26}=\alpha_{mC}\alpha_c\bar{\delta}^n\sin(\gamma)\sin\left(\kappa\left(\bar{\delta}^n\right)^2\right),$$

$$N_{31}=N_{32}=\alpha_{mh}\bar{\delta}^n,\quad N_{34}=-1,$$

$$N_{41}=\left(\cos\left(\bar{\delta}^n\right)+\bar{\delta}^n\sin\left(\bar{\delta}^n\right)-1\right)/\left(\bar{\delta}^n\right)^2-\alpha_I\bar{\delta}^n\sin\left(\bar{\delta}^n\right)-$$

$$\alpha_{mC}\left(\alpha_c\bar{\delta}^n\left(\cos(\gamma)+\alpha_c\right)\sin\left(\bar{\delta}^n\right)-\left(1+\alpha_c\cos(\gamma)\right)\cos\left(\bar{\delta}^n\right)\right),$$

$$N_{43}=\left(\sin\left(\bar{\delta}^n\right)-\bar{\delta}^n\cos\left(\bar{\delta}^n\right)\right)/\left(\bar{\delta}^n\right)^2+\alpha_I\bar{\delta}^n\cos\left(\bar{\delta}^n\right)+\alpha_{Ih}\bar{\delta}^n\left(1-\Omega_h^2\right)+$$

$$\alpha_{mC}\left(\alpha_c\bar{\delta}\left(\cos(\gamma)+\alpha_c\right)\cos\left(\bar{\delta}^n\right)+\left(1+\alpha_c\cos(\gamma)\right)\sin\left(\bar{\delta}^n\right)\right),$$

$$N_{44}=\left(\bar{\delta}^n\cosh\left(\bar{\delta}^n\right)-\sinh\left(\bar{\delta}^n\right)\right)/\left(\bar{\delta}^n\right)^2+\alpha_I\bar{\delta}^n\cosh\left(\bar{\delta}^n\right)+\alpha_{Ih}\bar{\delta}^n\left(1-\Omega_h^2\right)+$$

$$\alpha_{mC}\left(\alpha_c\bar{\delta}^n\left(\cos(\gamma)+\alpha_c\right)\cosh\left(\bar{\delta}^n\right)+\left(1+\alpha_c\cos(\gamma)\right)\sinh\left(\bar{\delta}^n\right)\right),$$

$$N_{45}=-\alpha_{mC}\alpha_c\sin(\gamma)\cos\left(\left(\bar{\delta}^n\right)^2\right),N_{46}=-\alpha_{mC}\alpha_c\sin(\gamma)\sin\left(\kappa\left(\bar{\delta}^n\right)^2\right),$$

$$N_{51}=-\alpha_{mC}\alpha_c\left(\bar{\delta}^n\right)^3\kappa\sin(\gamma)\sin\left(\bar{\delta}^n\right),N_{52}=\alpha_{mC}\alpha_c\left(\bar{\delta}^n\right)^3\kappa\sin(\gamma)\sinh\left(\bar{\delta}^n\right),$$

$$N_{53}=\alpha_{mC}\alpha_c\left(\bar{\delta}^n\right)^3\kappa\sin(\gamma)\cos\left(\bar{\delta}^n\right),N_{54}=\alpha_{mC}\alpha_c\left(\bar{\delta}^n\right)^3\kappa\sin(\gamma)\cosh\left(\bar{\delta}^n\right),$$

$$N_{55}=-\sin\left(\kappa\left(\bar{\delta}^n\right)^2\right)-\alpha_{mC}\left(\bar{\delta}^n\right)^2\kappa\cos\left(\kappa\left(\bar{\delta}^n\right)^2\right),$$

$$N_{56}=\cos\left(\kappa\left(\bar{\delta}^n\right)^2\right)-\alpha_{mC}\left(\bar{\delta}^n\right)^2\kappa\sin\left(\kappa\left(\bar{\delta}^n\right)^2\right),$$

$$N_{65}=\alpha_{mh}\left(\bar{\delta}^n\right)^2\kappa,\ N_{15}=N_{16}=N_{35}=N_{36}=N_{61}=N_{62}=N_{63}=N_{64}=0,\ N_{33}=N_{66}=1. \qquad (3.44)$$

The above elements have been expressed using the nondimensional parameters given in Eq. (3.11) along with $\alpha_{Ih}=I_h/\rho AL^3$, $\alpha_{mh}=m_h/\rho AL$, and $\Omega_h=\left(\left(k_\theta/I_h\right)/\omega_m^2\right)$. The determinant of the coefficient matrix i.e., $det\left|N\left(\bar{\delta}^n\right)\right|=0$, yields a transcendental equation known as eigenfrequency equation in terms of known dimensionless parameters. The mode shapes of manipulator are obtained by using the constants $\left(S_2....S_4,R_1,R_2\right)^n$ in Eq. (3.10) which are restructured by expressing the coefficients in term of ${S_1}^n$ of unit magnitude.

3.4.2 Position analysis

Rotational flexible robot has been assumed to have a smooth sinusoidal torque input of unit amplitude with a duty cycle of 2 seconds for a simulation period of 3 seconds to investigate the effect of offset parameters on its responses. The objective is to compute performance parameters i.e., overshoot and settling time that are effectively used to understand the controllability issues of flexible manipulators. It is essential to examine the influence of system parameters on the tip position to further develop effective control algorithms for a desired output. Hence, using assumed mode method $\left\{w(x,\tau)=W^1(x)q(t)\right\}$ and Eqs. (3.38) & (3.42), the dynamics of the link-hub system can be expressed in the form of matrices $[M]$, $[C]$, $[K]$, and $\left[F(t)\right]$, respectively representing the inertia, Coriolis and centripetal components, stiffness matrix and force vector as:

$$\left[M(q,\theta)\right]\ddot{q}+\left[C\left(q,\theta,\dot{q},\dot{\theta}\right)\right]\dot{q}+\left[K\left(q,\dot{\theta}\right)\right]q=\left[F(t)\right]. \tag{3.45}$$

3.4.3 Nonlinear forced vibration analysis

Similar to the linear analysis, here also the task to depict the effect of offset parameters on the system dynamics of a large deflection model of flexible manipulator with revolute joint is undertakenis examined. Considering the harmonic motion being imparted at the hub along with in-extensibility condition to highlight the longitudinal deformation as $u(x,t)=-(1/2)\int_0^x\left(\partial w/\partial x\right)^2 d\xi$, one may obtain the following equation of motion:

$$\begin{aligned}&\rho A[\ddot{w}-\left(\ddot{\theta}w_1+2\dot{w}\dot{\theta}+x\dot{\theta}^2\right)\left(-w'+\int_0^x w_{\xi\xi}d\xi\right)-w''\int_x^L\int_0^x\left(\dot{w}_\xi{}^2+\ddot{w}_\xi w_\xi\right)d\xi_1 d\xi_2-2\dot{\theta}\int_0^x w_\xi\dot{w}_\xi d\xi\\&-0.5\ddot{\theta}\int_0^x w_\xi{}^2 d\xi+w'\int_0^x\left(\dot{w}_\xi{}^2+\ddot{w}_\xi w_\xi\right)d\xi+x\ddot{\theta}-w\dot{\theta}^2-0.5\dot{\theta}^2(w'\int_0^x w_\xi{}^2 d\xi\\&-w''\int_x^L\int_0^x w_\xi{}^2 d\xi_1 d\xi_2)]+EI\left\{w''''+\left(w'\left(w'w''\right)'\right)'\right\}+c_d\dot{w}=0.\end{aligned} \tag{3.46}$$

Here, w_ξ represents the differentiation of w with respect to ξ. Using the dimensionless parameters: $\bar{w}=w/L, \bar{x}=x/L, \bar{\xi}_1=\xi_1/L, \tau=t\sqrt{EI/\rho AL^4}$, and $\bar{c}=c_d L^2/\sqrt{\rho AEI}$, one may obtain the following dimensionless temporal equation of motion as:

$$\begin{aligned}&\bar{w}''''+\left(\overline{w'}\left(\overline{w'w''}\right)'\right)'+\bar{c}\dot{\bar{w}}+\ddot{\bar{w}}+\bar{x}\ddot{\bar{\theta}}-\bar{w}\dot{\bar{\theta}}^2+\overline{w'}\int_0^{\bar{x}}\left(\dot{\bar{w}}_{\bar{\xi}}{}^2+\ddot{\bar{w}}_{\bar{\xi}}\bar{w}_{\bar{\xi}}\right)d\bar{\xi}-\overline{w''}\int_{\bar{x}}^1\int_0^{\bar{x}}\left(\dot{\bar{w}}_\xi{}^2+\ddot{\bar{w}}_{\bar{\xi}}\bar{w}_{\bar{\xi}}\right)d\bar{\xi}_1 d\bar{\xi}_2\\&-\left(\ddot{\bar{\theta}}\bar{w}_1+2\dot{\bar{w}}\dot{\bar{\theta}}+\bar{x}\dot{\bar{\theta}}^2\right)\left(-\overline{w'}+\int_0^{\bar{x}}\bar{w}_{\bar{\xi}\bar{\xi}}d\bar{\xi}\right)-2\dot{\bar{\theta}}\int_0^{\bar{x}}\bar{w}_{\bar{\xi}}\dot{\bar{w}}_{\bar{\xi}}d\bar{\xi}-0.5\ddot{\bar{\theta}}\int_0^{\bar{x}}\bar{w}_{\bar{\xi}}{}^2 d\bar{\xi}-\\&0.5\dot{\bar{\theta}}^2\left(\overline{w'}\int_0^{\bar{x}}\bar{w}_{\bar{\xi}}{}^2 d\bar{\xi}-\overline{w''}\int_{\bar{x}}^1\int_0^{\bar{x}}\bar{w}_{\bar{\xi}}{}^2 d\bar{\xi}_1 d\bar{\xi}_2\right)=0.\end{aligned} \tag{3.47}$$

The spatio-temporal Eq. (3.47) is then discretized into dimensionless temporal equation using Galerkin's method by replacing $\bar{w}(\bar{x},\tau)$ with $r\psi(\bar{x})p(\tau)$ where r, $\psi(\bar{x})$, $p(\tau)$ are the scaling factor, admissible function obtained by satisfying associated boundary conditions, and time modulation, respectively. Further, applying the orthogonal property of the mode shapes, one may obtain the governing temporal equation of motion of manipulator after ordering the terms as:

$$\begin{aligned}&\ddot{p}(\tau)+\bar{\Omega}^2 p(\tau)+2\varepsilon\xi\dot{p}(\tau)+\varepsilon\alpha_1 p^3+\varepsilon\alpha_2 p\dot{p}^2+\varepsilon\alpha_3 p\ddot{p}+\left\{\alpha_4 p^2\cos(\omega\tau)+\alpha_5 p\dot{p}\sin(\omega\tau)\right\}\\&-\varepsilon\left\{\alpha_6 p\sin^2(\omega\tau)+\alpha_7\cos(\omega\tau)+\alpha_8 p^3\sin^2(\omega\tau)\right\}=0.\end{aligned} \tag{3.48}$$

The above equation is found to be highly nonlinear, thus, approximate solution is highly anticipated and this closed form approximate solution to the Eq. (3.48) is sought here by exploring the method of multiple scales where, the displacement has been expressed in terms of various times scales such as $T_n=\varepsilon^n\tau$, (n = 0, 1), in the following form:

$$p=p_1(T_0,T_1)+\varepsilon p_2(T_0,T_1). \tag{3.49}$$

Now, p is determined as a function of these time scales instead of τ. After substituting, the coefficients of the same powers of ε are equated to obtain the following equations:

$$O\left(\varepsilon^1\right):\ \partial^2 p_1/\partial T_0{}^2+\bar{\Omega}^2 p_1=0 \tag{3.50}$$

$$\partial^2 p_2/\partial T_0{}^2+2\left(\partial^2 p_1/\partial T_0\partial T_1\right)+\bar{\Omega}^2 p_2+2\xi\left(\partial p_1/\partial T_0\right)+\alpha_1 p_1^3+\alpha_2 p_1\left(\partial p_1/\partial T_0\right)^2$$

$$\mathrm{O}\left(\varepsilon^2\right):\ +\alpha_3 p_1^2\left(\partial^2 p_1/\partial T_0^2\right)+\alpha_4 p_1^2\cos\left(\omega T_0\right)+\alpha_5 p_1\left(\partial p_1/\partial T_0\right)\sin\left(\omega T_0\right)-\alpha_6 p_1\sin^2\left(\omega T_0\right) \tag{3.51}$$

$$-\alpha_7\cos\left(\omega T_0\right)-\alpha_8 p_1^3\sin^2\left(\omega T_0\right)=0.$$

The general solution of Eq. (3.50) can be expected as:

$$p_1=B(T_1)\exp\left(i\bar{\Omega}T_0\right)+\bar{B}(T_1)\exp\left(-i\bar{\Omega}T_0\right). \tag{3.52}$$

Substituting Eq. (3.52) into Eq. (3.51) gives:

$$\partial^2 p_2/\partial\mathrm{T}_0{}^2+\bar{\Omega}^2 p_2+2\mathrm{i}\,\bar{\Omega}\left(\partial B/\partial\mathrm{T}_1\right)\exp\left(i\bar{\Omega}T_0\right)+2\xi\mathrm{i}\,\bar{\Omega}\ \mathrm{B}\exp\left(i\bar{\Omega}T_0\right)-\alpha_1 B^3\exp\left(3i\bar{\Omega}T_0\right)$$
$$-\alpha_2\bar{\Omega}^2\left(B^3\exp\left(3i\bar{\Omega}T_0\right)-B^2\bar{B}\exp\left(i\bar{\Omega}T_0\right)\right)-\alpha_3\bar{\Omega}^2\left(B^3\exp\left(3i\bar{\Omega}T_0\right)+3B^2\bar{B}\exp\left(i\bar{\Omega}T_0\right)\right)-$$
$$0.5\alpha_7\exp\left(i\omega T_0\right)+0.5\alpha_4\left(B^2\exp i\left(2\bar{\Omega}+\omega\right)T_0+\bar{B}^2\exp i\left(\omega-2\bar{\Omega}\right)T_0+2B\bar{B}\exp i\left(\omega\right)T_0\right)+$$
$$0.5\alpha_5\bar{\Omega}\left(B^2\exp i\left(2\bar{\Omega}+\omega\right)T_0-\bar{B}^2\exp i\left(\omega-2\bar{\Omega}\right)T_0\right)-\alpha_8\left\{B^3\exp\left(3i\bar{\Omega}T_0\right)-3B^2\bar{B}\exp\left(i\bar{\Omega}T_0\right)\right\}+$$
$$\left\{0.5\left(B^3\exp i\left(3\bar{\Omega}+2\omega\right)T_0+\bar{B}^3\exp i\left(2\omega-3\bar{\Omega}\right)T_0+3B^2\bar{B}\exp i\left(\bar{\Omega}-2\omega\right)T_0\right)\right\}-$$
$$3\alpha_1 B^2\bar{B}\exp\left(i\bar{\Omega}T_0\right)-0.5\alpha_6\left\{B\exp\left(i\bar{\Omega}T_0\right)-0.5\left(B\exp i\left(\bar{\Omega}+2\omega\right)T_0+\bar{B}\exp i\left(2\omega-\bar{\Omega}\right)T_0\right)\right\}+cc=0. \tag{3.53}$$

Any solution from the above equation may lead to an unbounded solution when the small divisor and secular terms are being included in the solution. The terms associated with $\exp\left(\pm i\bar{\Omega}T_0\right)$, $\exp\pm i\left(2\omega-3\bar{\Omega}\right)T_0$, and $\exp\pm i\left(\omega-2\bar{\Omega}\right)T_0$ are known as small divisor and secular terms. These terms needed have to be eliminated in order to obtain any bounded or finite solution. It may be observed that these terms exist when ω nearly equals either to $\bar{\Omega}$, i.e., simple resonance condition, or $3\bar{\Omega}$, i.e., sub-harmonic condition. These two cases are studied in the following sub-sections in detail.

3.4.4 Primary resonance case: $\left(\omega\approx\bar{\Omega}\right)$

Nearness of ω to $\bar{\Omega}$ is expressed as $\bar{\Omega}+\varepsilon\sigma_1$ by using detuning parameter σ_1 for primary resonance condition, i.e., rotating frequency (ω) becomes nearly equal to normalized natural frequency of the system $\left(\bar{\Omega}\right)$. Replacing ω with $\bar{\Omega}+\varepsilon\sigma_1$ into Eq. **Error! Reference source not found.**, yields an equation involving both secular and non-secular terms. In order to obtain the bounded solution of the Eq. (3.53), the terms proportional to $\exp\left(\pm i\bar{\Omega}T_0\right)$ leading to secular terms in the particular solution are eliminated as:

$$2\mathrm{i}\,\bar{\Omega}\left(\partial B/\partial\mathrm{T}_1\right)+2\xi i\bar{\Omega}\,B+\left(3\alpha_1+\alpha_2\bar{\Omega}^2-3\alpha_3\bar{\Omega}^2-3\alpha_8\right)B^2\bar{B}-\alpha_6 B/2+$$
$$\left(\alpha_4/2-\alpha_5\bar{\Omega}/2\right)B^2\exp\left(-i\sigma_1T_1\right)+\left(\alpha_4B\bar{B}-\alpha_7/2\right)\exp\left(i\sigma_1T_1\right)+ \tag{3.54}$$
$$\left(\alpha_6\bar{B}/4+3\alpha_8\bar{B}^2B/2\right)\exp\left(2i\sigma_1T_1\right)+\left(\alpha_8/4\right)B^3\exp\left(-2i\sigma_1T_1\right)=0.$$

Now substituting $B\left(T_1\right)$ in polar form as $B=(1/2)b_1(T_1)e^{i\beta_1(T_1)}$ and separating real and imaginary terms, one may obtain following reduced autonomous equations:

$$\bar{\Omega}b_1' = -\xi\bar{\Omega}b_1 + \left(\alpha_4/8 - \alpha_5\bar{\Omega}/8\right)b_1^2\sin(\lambda_1) + \left(\alpha_8 b_1^3/16\right)\sin(2\lambda_1) - \left(\alpha_4 b_1^2/4 - \alpha_7/2\right)\sin(\lambda_1)$$
$$-\left(\alpha_6 b_1/8 + 3\alpha_8 b_1^3/16\right)\sin(2\lambda_1) = 0,$$
$$b_1\bar{\Omega}\lambda_1' = b_1\bar{\Omega}\sigma_1 - \left(3\alpha_1 + \alpha_2\bar{\Omega}^2 - 3\alpha_3\bar{\Omega}^2 - 3\alpha_8\right)\left(b_1^3/8\right) + \alpha_6 b_1/4 - \left(\alpha_4/8 - \alpha_5\bar{\Omega}/8\right)b_1^2\cos(\lambda_1) -$$
$$\left(\alpha_4 b_1^2/4 - \alpha_7/2\right)\cos(\lambda_1) - \left(\alpha_6 b_1/8 + 3\alpha_8 b_1^3/16\right)\cos(2\lambda_1) + \left(\alpha_8 b_1^3/16\right)\cos(2\lambda_1) = 0,$$
$$\lambda_1 = \sigma_1 T_1 - \beta_1. \tag{3.55}$$

However, the first order solution for the time responses of manipulator in terms of original variable τ is given as.

$$p = (1/2)b_1\cos(\omega\tau - \lambda_1) + O(\varepsilon). \tag{3.56}$$

The stability of the steady-state solutions of Eq. (3.55) is investigated by examining the eigenvalues of the Jacobian matrix *[J]* as explained in section 3.1.3. The elements of the matrix *[J]* are given as:

$$J_{11} = -\xi - \left(\alpha_4/4\bar{\Omega} - \alpha_5/4\right)b_{10}\sin(\lambda_{10}) - \left(\alpha_6/8\,\bar{\Omega}\right)\sin(2\lambda_{10}) - \left(3\alpha_8/4\bar{\Omega}\right)b_{10}^2\sin(2\lambda_{10}),$$
$$J_{12} = -\left(\alpha_4/8\,\bar{\Omega} - \alpha_5/8\right)b_{10}^2\cos(\lambda_{10}) + \left(\alpha_7/2\,\bar{\Omega}\right)\cos(\lambda_{10}) - \left(\alpha_6 b_{10}/4\,\bar{\Omega}\right)\cos(2\lambda_{10}) -$$
$$\left(\alpha_8/4\bar{\Omega}\right)b_{10}^3\cos(2\lambda_{10}),$$
$$J_{13} = \sigma_2/b_{10} - 3\left(3\alpha_1 + \alpha_2\bar{\Omega}^2 - 3\alpha_3\bar{\Omega}^2 - 3\alpha_8\right)b_{10}/8\bar{\Omega}\alpha_6/4b_{10}\bar{\Omega} - \left(3\alpha_4/4\,\bar{\Omega} - \alpha_5\bar{\Omega}/4\right)\cos(\lambda_{10}) -$$
$$\left(\alpha_6/8b_{10}\bar{\Omega}\right)\cos(2\lambda_{10}) - \left(3\alpha_8 b_{10}/4\bar{\Omega}\right)\cos(2\lambda_{10}),$$
$$J_{14} = \left(3\alpha_4/8\,\bar{\Omega} - \alpha_5\bar{\Omega}/8\right)b_{10}\sin(\lambda_{10}) - \left(\alpha_7/2b_{10}\bar{\Omega}\right)\sin(\lambda_{10}) + \left(\alpha_6/4\bar{\Omega}\right)\sin(2\lambda_{10}) +$$
$$\left(\alpha_8 b_{10}^2/2\,\bar{\Omega}\right)\sin(2\lambda_{10}). \tag{3.57}$$

3.4.5 Subharmonic resonance case: $\left(\omega \approx 3\bar{\Omega}\right)$

Using a procedure identical to that discussed in the previous section, one may obtain the following reduced equations in autonomous form.

$$b_2\bar{\Omega}\lambda_2' = b_2\bar{\Omega}\sigma_2 - \left(3\alpha_1 + \alpha_2\bar{\Omega}^2 - 3\alpha_3\bar{\Omega}^2 - 3\alpha_8\right)\left(3b_2^3/8\right) + 3\alpha_6 b_2/4 - \left(\alpha_4 - \alpha_5\bar{\Omega}\right)3b_2^2\cos(\lambda_2)/8 = 0,$$
$$\bar{\Omega}b_2' = -\xi\bar{\Omega}\,b_2 - \left(\alpha_4/8 - \alpha_5\bar{\Omega}/8\right)b_2^2\sin(\lambda_2) = 0. \tag{3.58}$$

The first order nontrivial solution for the time response of manipulator is given by

$$p = (1/2)b_2\cos(\omega\tau - \lambda_2)/3 + O(\varepsilon). \tag{3.59}$$

For the steady-state condition, the left hand side of Eq. (3.58) becomes zero and the system renders both trivial $(b_2 = 0)$ and nontrivial $(b_2 \neq 0)$ solutions and the frequency response equation can be obtained by eliminating the phase (λ_2) from the resulting equations. The stability of nontrivial solutions is then investigated by similar procedure as explained in previous section.

3.4.6 Numerical results and discussion

a) *Modal analysis: eigenspectrums*

The modal parameters as a pre-requisite to further characterize the resonant vibration in machinery and structures are computed. Usually, any mode of vibration is defined by the modal parameters, i.e., natural frequency, mode shape, and modal damping. Hence, estimation of those parameters is important in understanding of the overall dynamics of the system. Fig. 3.16-Fig. 3.17 show the characteristics behavior of eigenfrequency with system parameters. Here, eigenfrequencies and corresponding eigenfunctions have been evaluated by considering both transverse and axial deformation. From Fig 3.16, it is evident that the eigenfrequency de-

creases as the payload mass (α_{mC}) increases. Similarly, for a specific value of payload mass, the system eigenfrequencies decrease with increasing of payload inertia (α_I) .

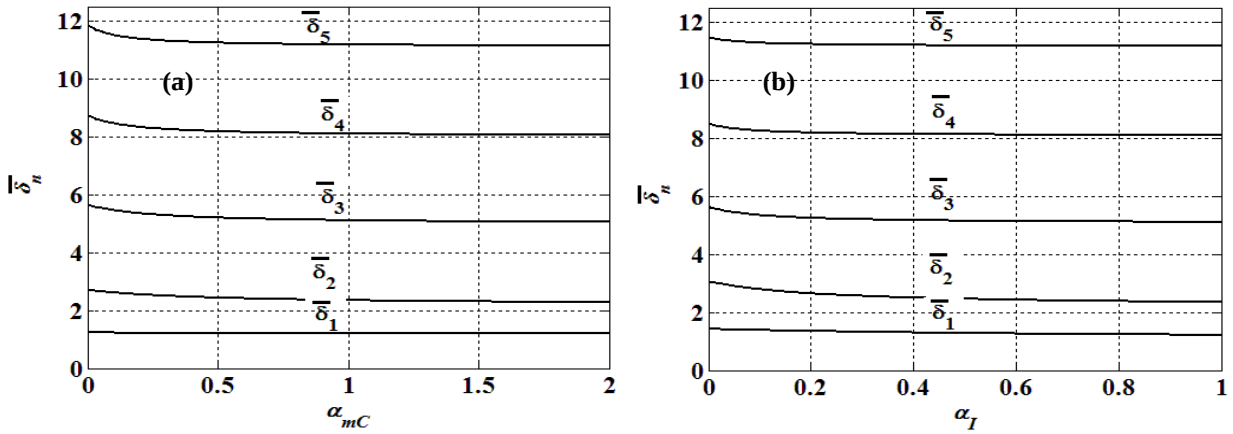

Fig. 3.16: Variation of eigenfrequencies with (a) payload mass and (b) inertia parameters for α_{mh} =1.0, α_{Ih} =1.0, Ω_h =0.5, α_c =0.5, $\gamma = 30^o$.

It is also observed that the eigenfrequency decreases when the hub mass (α_{mh}) and inertia (α_{Ih}) of rotating hub are increased. The eigenfrequencies for the R-F beam calculated by [Coleman and McSweeney, 2004] can also be determined from the present model by eliminating the dynamics of hub, payload and axial deformation. With these observations, it is evident that with increase in mass and inertia of payload or actuator, increases the overall effective inertia of the system and as a result, the natural frequency gets decreased $\left(\omega_n \propto \sqrt{K/M}\right)$ with increase in all those parameters.

The effect of offset-ratio (α_c) and hub frequency parameter (Ω_h) on the eigenfrequencies can be inferred from Fig. 3.17. It is observed that only the higher eigenfrequencies increase with the increase in offset ratio (α_c) . Hence, it becomes imperative to control the lower eigenfrequencies for efficient control of manipulator to achieve the desired position when the manipulator is lifting a payload which is having its centre of gravity different than the terminal point of the link. The hub frequency parameter (Ω_h) is varied by regulating the value of the stiffness of actuator while keeping all other parameters constant. It is noticed that for the lower value of hub stiffness $(\Omega_h < 1)$, the eigenfrequencies are found to be increased. A sudden jump is observed when the rotating frequency becomes equal to that of fundamental natural frequency $(\Omega_h = 1)$. With further increase in frequency parameter, natural frequency appears to be remain constant.

The eigenspectrums of first two modes of vibrations for four different models of flexible link manipulator are compared in Fig. 3.18. The first case corresponds to the mode shape obtained in [Coleman and McSweeney, 2004] for R-F beam case; second case represents the condition when the dynamics of the hub is neglected; in the third case the axial motion of the manipulator is neglected but include the hub motion; and finally the manipulator is described considering the axial as well as the hub motion of the link. It can be concluded that the consideration of axial motion in the analysis significantly increases the amplitude of the end-effector in all modes of vibrations.

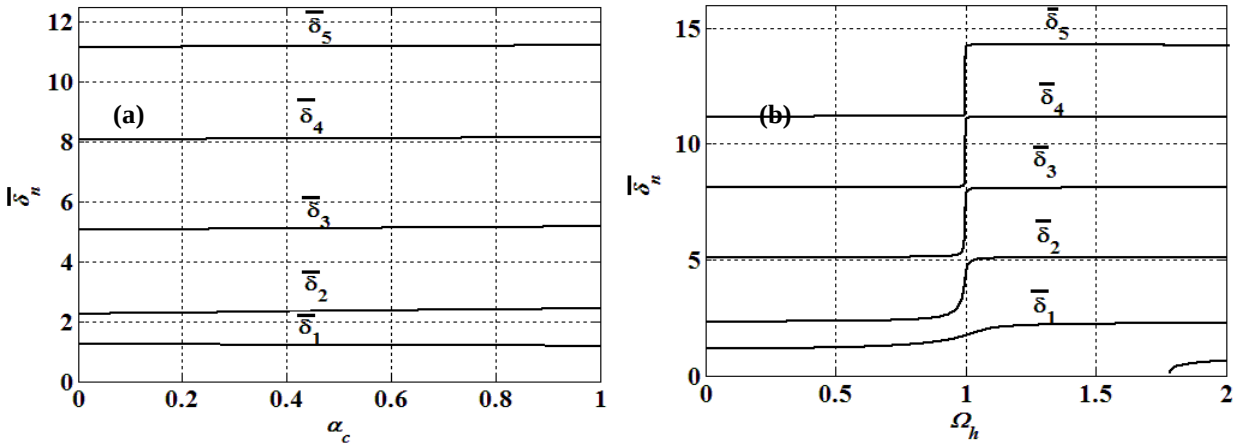

Fig. 3.17: Variation of eigenfrequencies with (a) offset ratio and (b) joint frequency parameter for α_{mC} =1.0, α_I =1.0, α_{mh} =1.0, α_{Ih} =1.0, $\gamma = 30^o$.

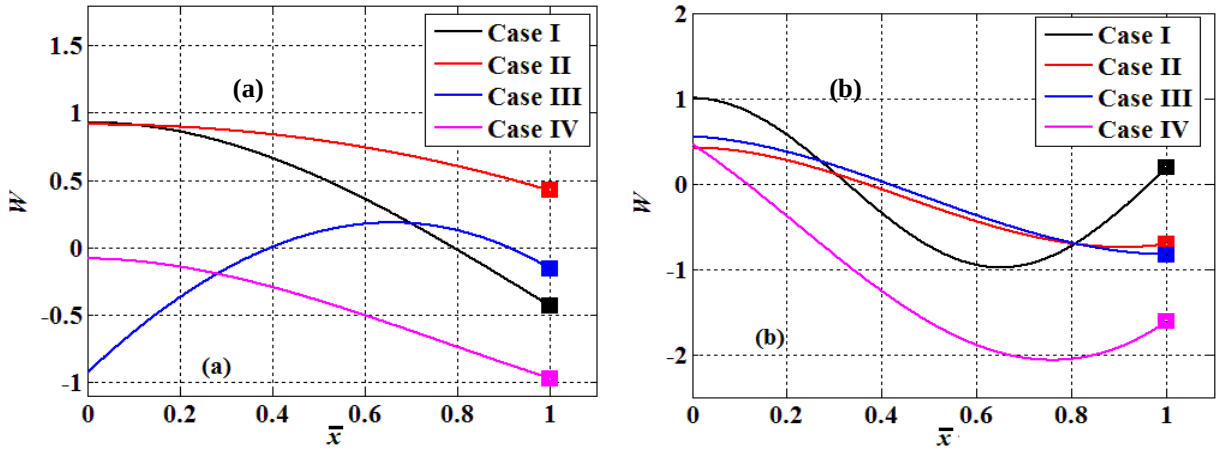

Fig. 3.18: Comparison of mode shapes for four different models (a) mode 1 (b) mode 2.

Variation of mode shapes of manipulator with payload mass is shown in Fig. 3.19 and it is observed that the node shifts towards the payload end with the increase in payload mass (α_{mC}) and effect of payload is significant in case of first mode of vibration. It can also be noticed that the payload leads to the significant deflection as compared to zero payload condition; this is because of the fact that the axial motion gets decoupled from the transverse vibration for zero payload. It is obvious from the Fig. 3.20 that the increase in hub mass (α_{mh}) significantly increases the deflection at actuator as well as payload end for almost all modes of vibration. The payload inertia (α_I) primarily affects the first few modes of vibration shown in Fig. 3.21.

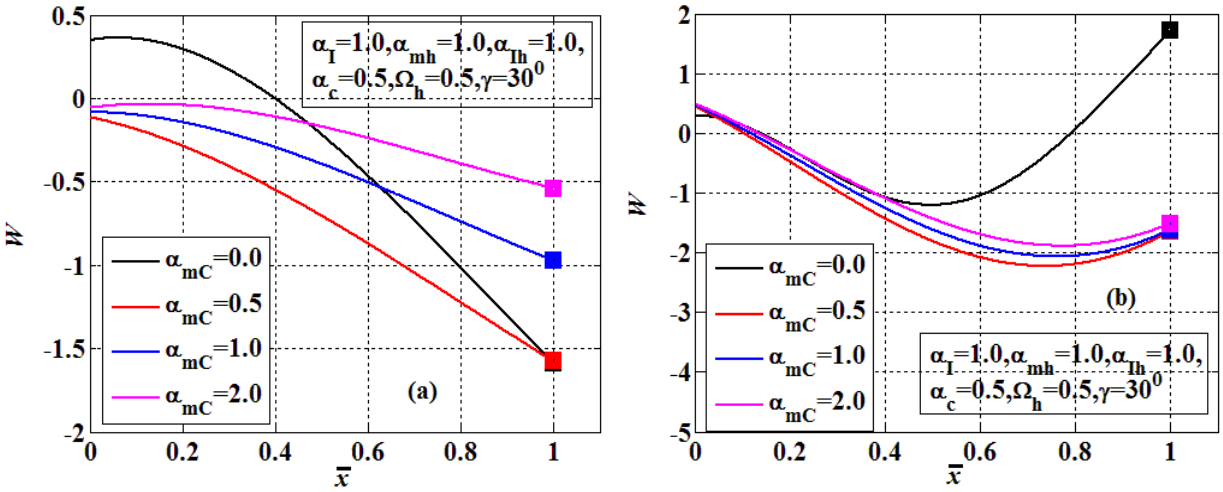

Fig. 3.19: Variation of mode shapes with offset mass (α_{mC}) (a) mode 1 (b) mode 2.

From Fig. 3.22 it is observed that for Ω_h < 1, deflection at the actuator end decreases significantly with the hub frequency parameter (Ω_h) for lower modes of vibration. For Ω_h = 1, the manipulator vibrates with a mode higher than the mode corresponding to the hub frequency parameter value lower than unity which is has also been shown in Fig. 3.17. A marginal influence on the amplitudes of the both ends of manipulator is noticed with the further increase in hub frequency parameter (Ω_h).

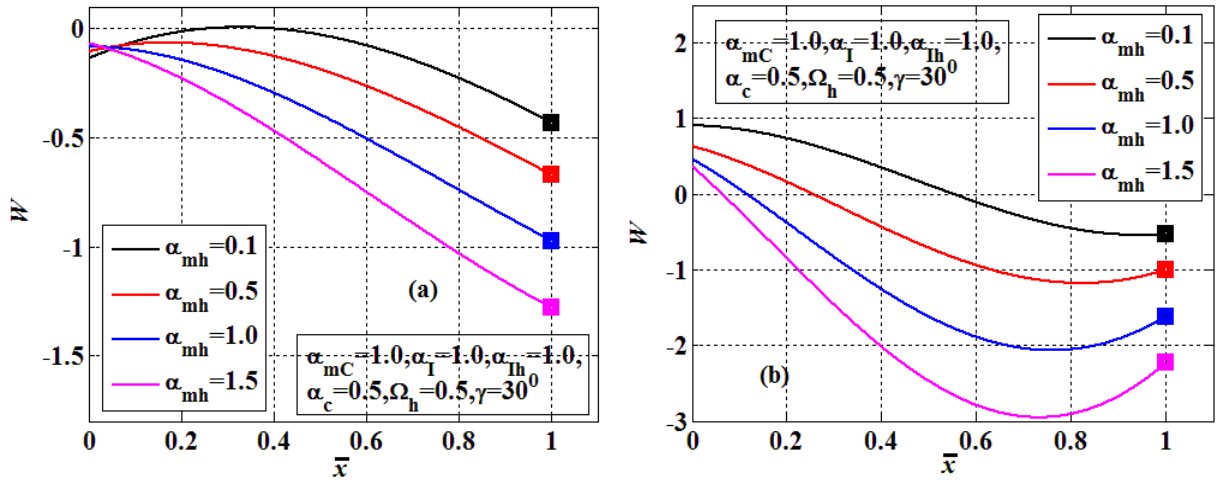

Fig. 3.20: Variation of mode shapes with hub mass (α_{mh}) (a) mode 1 (b) mode 2.

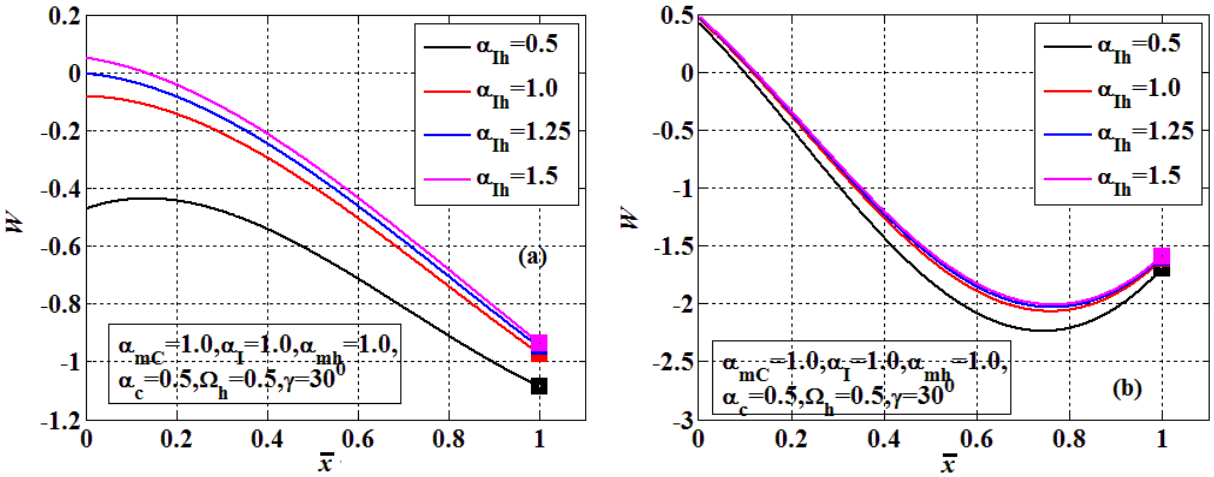

Fig. 3.21: Variation of mode shapes with payload inertia (α_I) (a) mode 1 (b) mode 2.

In Fig. 3.23, the comparison has been made with the condition when the payload is fixed at the point of attachment with zero offset, i.e., point payload. A large defleclion in the manipulator with paylaod is noticed as compared to the no payload condition. It is obtained that the increase in offset ratio (α_c) increases the amplitude of the modal displacement especially for the lower modes of vibrations. It ishas observed that offset payload may offer an actual and realistic modal displacement, while considering point payload may turn into a minimum 40-50% erroneous prediction as compared to a generic payload. Thus, for forecasting the actual dynamic response and its key role onto the structural stability, it is inevitable to encapsulate the offset conditions associated with payload.

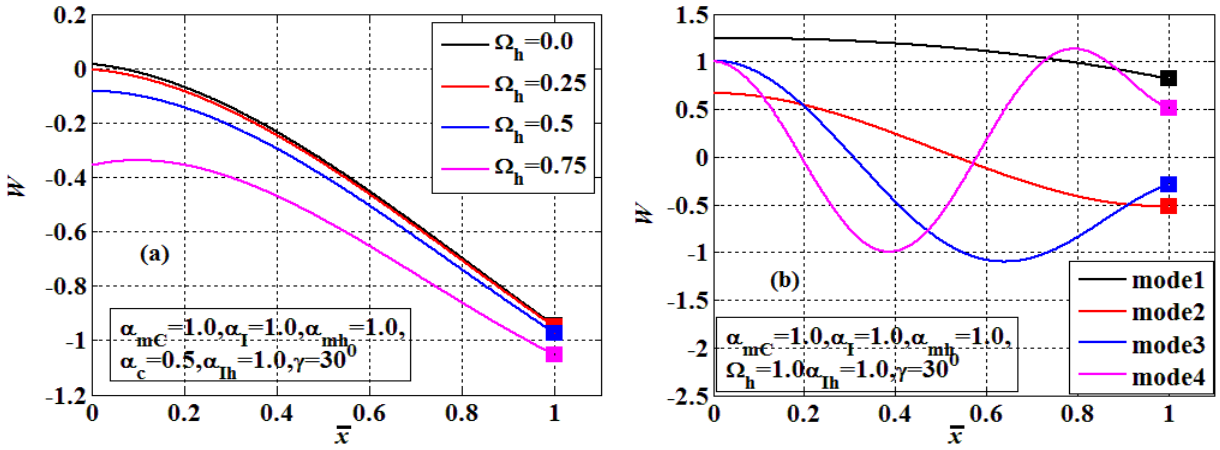

Fig. 3.22: Variation of mode shapes with hub frequency parameter (a) $\Omega_h < 1$ (b) $\Omega_h = 1$.

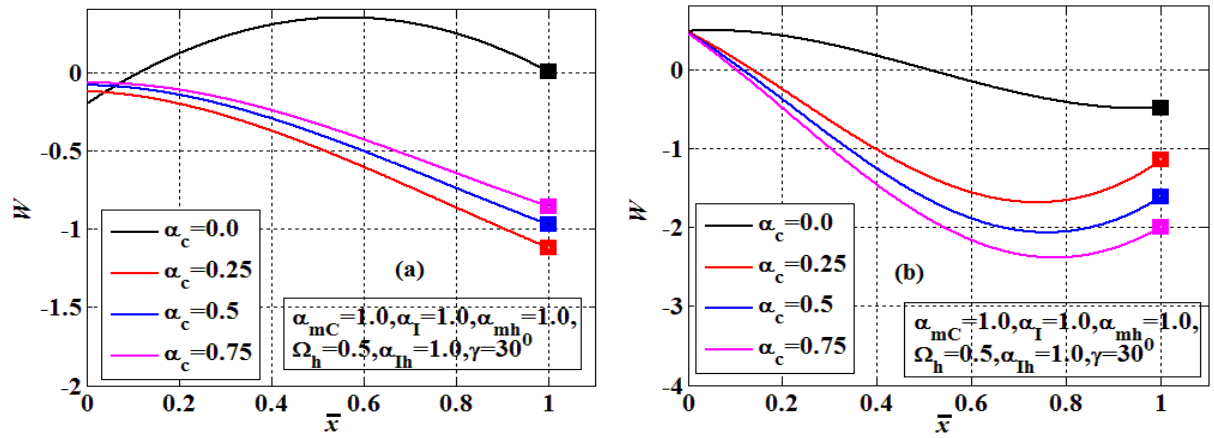

Fig. 3.23: Variation of mode shapes with offset ratio (α_c) (a) mode 1 (b) mode 2.

b) *System performance: tip Responses*

The structural flexibility in links and joints of a robotic system often gives rise a problem in end-point positioning inaccuracy while practically this position inaccuracy needs to be damped out or controlled to achieve desired performance. Thus, the performance parameters have been evaluated here to demonstrate how the structural parameters affect the tip position for a given motion. Dynamic performances of the system in the sense to reach its final state or delaying the overall system responses has been evaluated from Eq. (3.45) with an applied smooth sinusoidal torque at rotating hub. Here, the dynamic response has been obtained for the system with young's modulus E=210 Gpa, and mass density of $\rho = 7800$ kg/m^3, hub mass moment of inertia and mass of I_a = 20x10^{-4} kgm^2 and 0.1 kg, respectively. The payload at the terminal end of the manipulator is having only axial offset. The variation of tip displacement (m) and angular tip position (rad) with payload parameters, i.e., payload mass, payload inertia and offset length has been demonstrated in Fig. 3.24. It has been observed that the tip position and overshoot decreases with the increase in payload mass. Also, the settling time decreases from 0.75 s to 5 s as the payload mass is increased from 0.1 kg to 0.3 kg. Angular position of the link for three values of payload, i.e., 0.1 kg, 0.2 kg and 0.3 kg, respectively, are 0.19 rad, 0.13 rad and 0.90 rad.

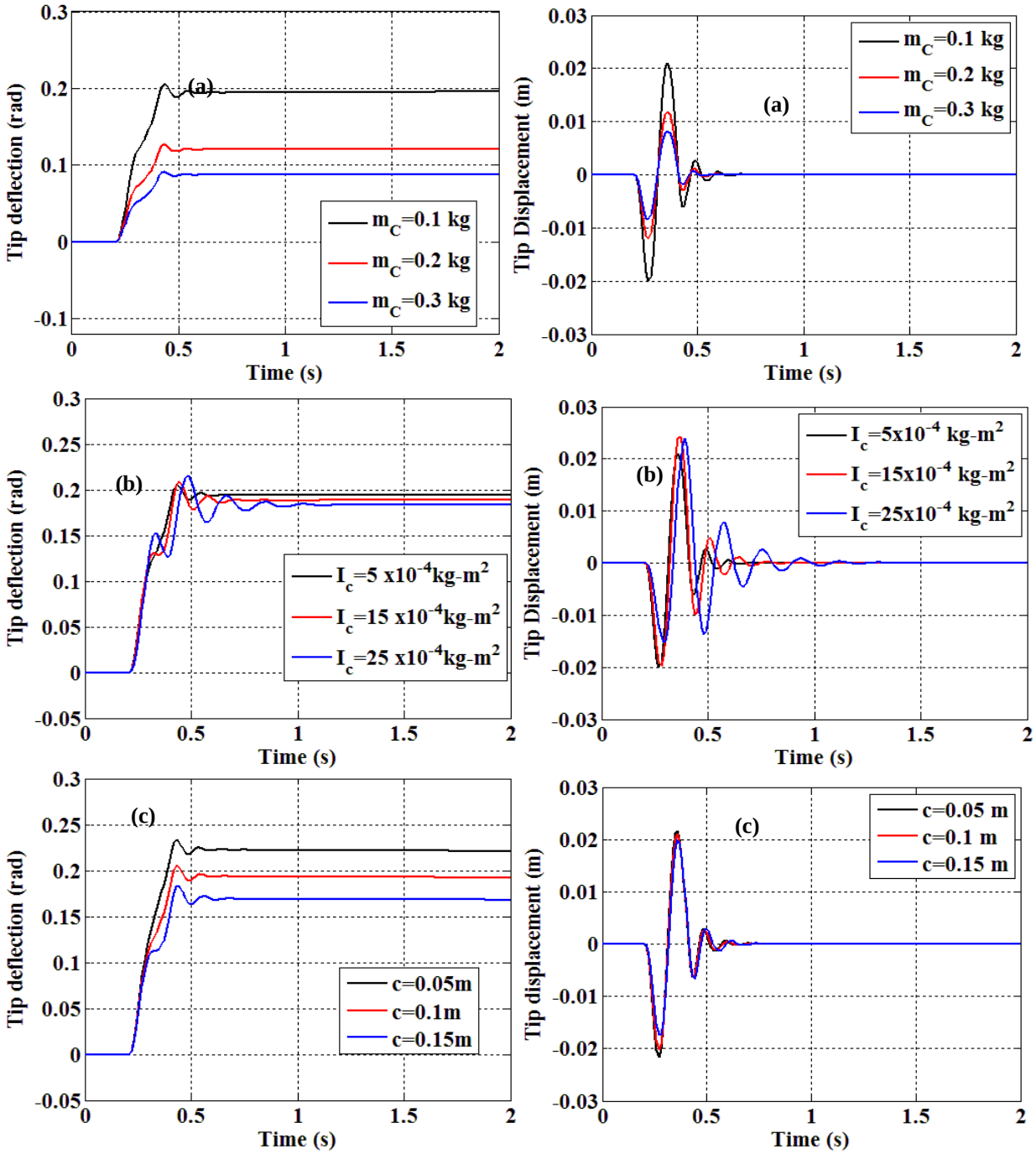

Fig. 3.24: Variation of manipulator tip deflections and modal displacements with (a) payload mass (b) payload inertia (c) payload offset.

c) *Nonlinear analysis: bifurcation and stability*

For all numerical simulations, the beam with length $L=0.35$ m, width $b=0.03$ m, height $h=0.003$ m has been considered while small-parameter ε, and scaling factor *(r)* are selected as 0.1 and 0.1, respectively. The damping coefficient *(ξ)* and amplitude ratio (θ_0) are chosen as 0.1, and 0.005 for primary resonance while these values for subharmonic resonance case are 0.001 and 0.05, respectively. The effect of parametric variations of these offset variables on the nonlinear behavior and assessment of stability under primary and secondary resonance conditions has been demonstrated. Frequency response curves in Fig. 3.25 depict the presence of jump phenomena due to S-N bifurcation for the primary resonance case and subharmonic resonance case because of geometric and inertial nonlinearities resulting in multiple solutions. The solid line represents the stable solutions, while dashed line depicts the unstable solutions

in all frequency response curves. In both the cases, the frequency response curve is bent towards left as the system reveals spring softening behavior. For first case, jump up and jump down has been found at point B and E, respectively when a slight increase or decrease in frequency takes place at these points. In second case, when frequency is at the critical point I, the system experiences a saddle-node bifurcation and the response amplitude jumps down to the stable trivial response in point J. A sudden decrease in amplitude due to this jump may cause a catastrophic structural failure. This can be avoided by operating the system in safe zones depicted in response curves.

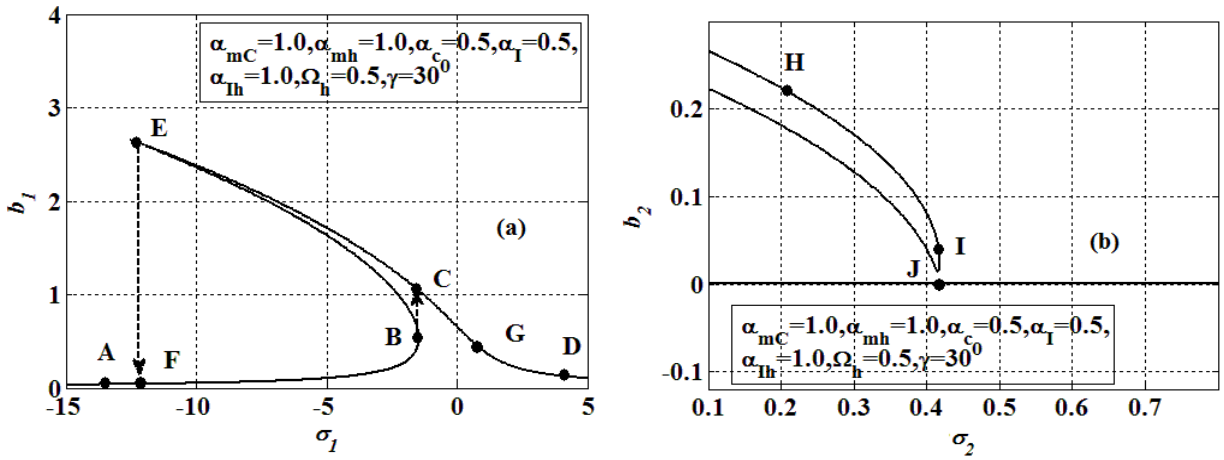

Fig. 3.25: Frequency response curves for flexible robotic manipulator for (a) primary and (b) sub-harmonic resonance.

The approximate solution is being validated with the findings obtained numerically using time responses, and phase portrait at three critical points C, G, D marked in frequency response characteristics for primary resonance in Fig. 3.26. The results obtained analytically are in good agreement with those obtained by numerically integrating Eq. (3.48).

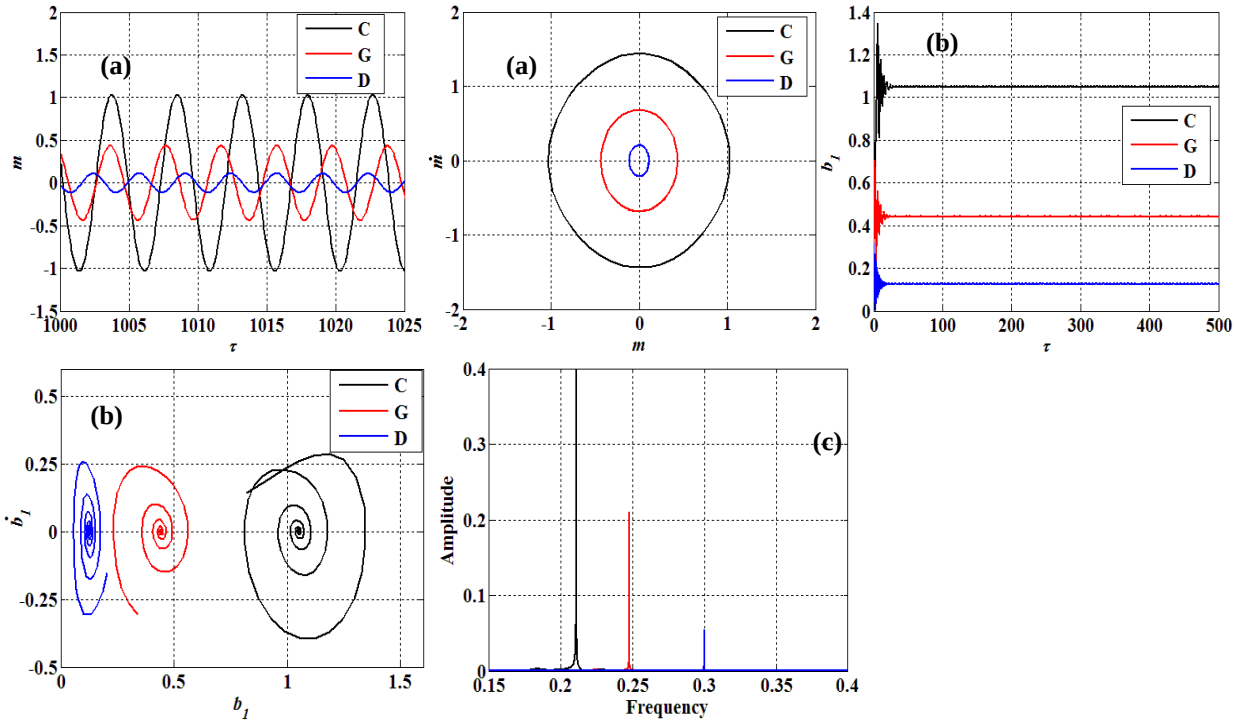

Fig. 3.26: Analytical (a) numerical (b) time history, phase portrait, and FFT (c) of critical points C, G, and D identified in Fig. 3.2 for primary resonance case.

The effect of offset mass (α_{mC}) on the frequency response curves is illustrated in Fig. 3.27. In primary resonance case, the amplitude of the manipulator increases with the increase in payload mass. The bi-stable region also increases without affecting the jump length with increase in payload mass for subharmonic resonance condition. In addition, it is noticed that for higher payload mass, the jump down phenomenon occurs at much lower frequency of the pulsating force. Thus, the system instability can be regulated by adjusting the value of payload mass yielding minimum jump length.

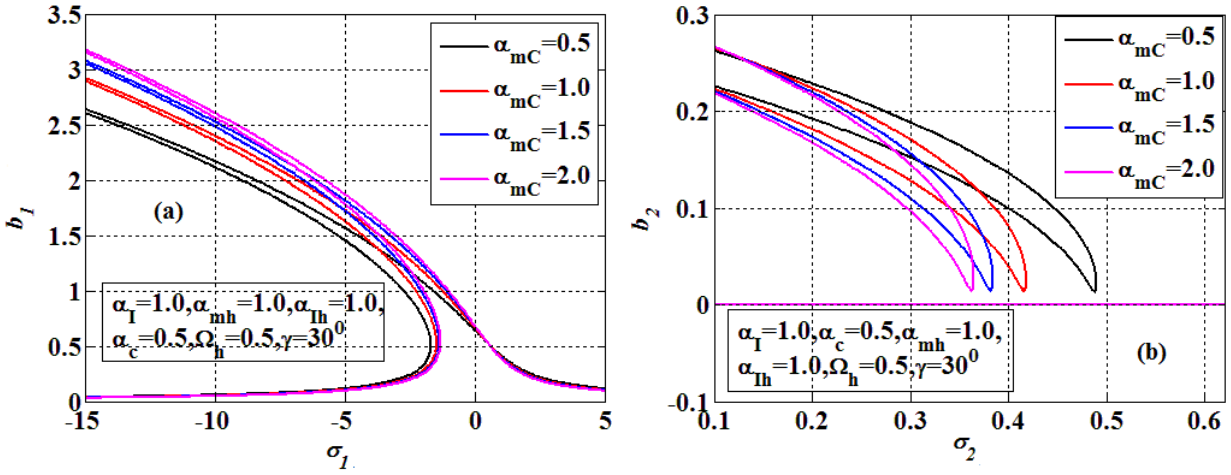

Fig. 3.27: Variation frequency response curves with payload mass (α_{mc}) for (a) primary and (b) sub-harmonic resonance.

The influence of payload inertia (α_I) on the system stability is depicted in Fig. 3.28. The increase in payload inertia decreases the jump length and consequently the maximum amplitude of the system decreases for primary resonance case. However the bi-stable region in subharmonic resonance case significantly increases without changing the jump length with increase in payload inertia.

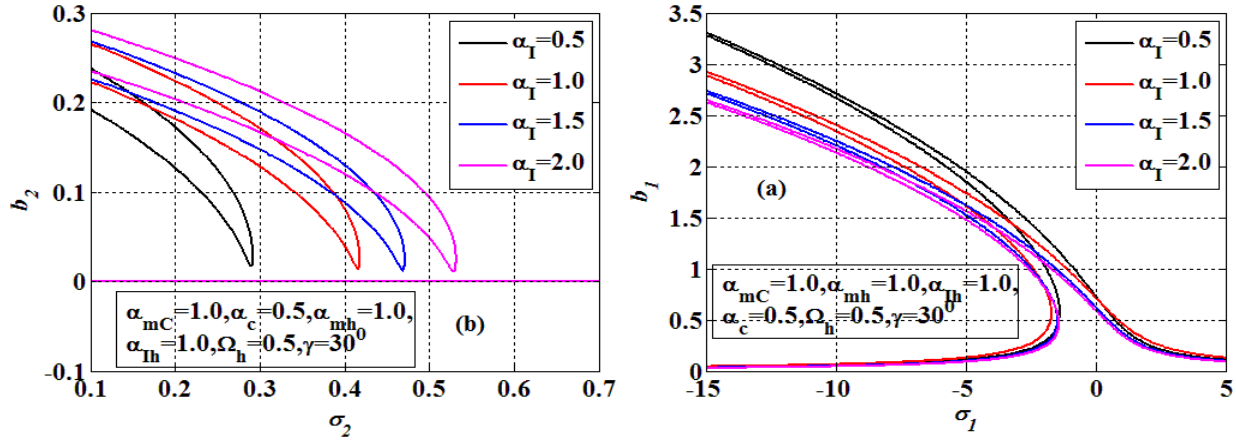

Fig. 3.28: Variation frequency response curves with payload inertia (α_I) for (a) primary and (b) sub-harmonic resonance.

From Fig. 3.29, an increase in vibration amplitude is noticed with the increase in hub inertia (α_{Ia}) with a significant effect on bi-stable region in the frequency response curve of subharmonic resonance case. The jump length is observed to be increased with increase in hub inertia and the jump-down phenomena starts at much lower frequency for large hub inertia. It is evident from Fig. 3.30 that, in case of primary resonance, the maximum amplitude of the system decreases as the center of gravity moves away from the point of attachment. The increase in offset ratio also increases the bi-stable region in subharmonic resonance case. Hence, more

offset distance becomes more vulnerable to catastrophic failure due to its elevated instability range.

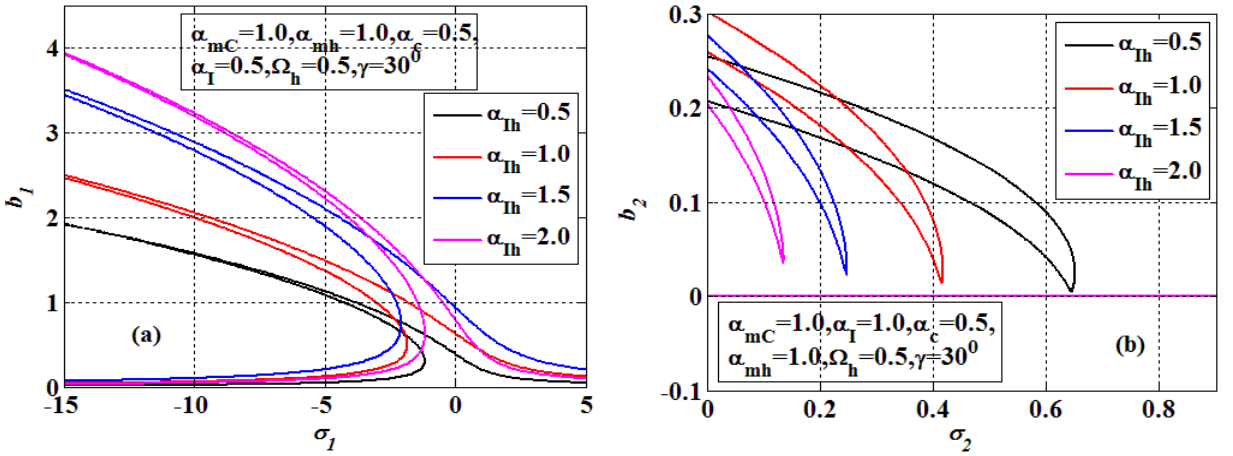

Fig. 3.29: Variation frequency response curves with actuator inertia (α_{Ih}) for (a) primary and (b) sub-harmonic resonance.

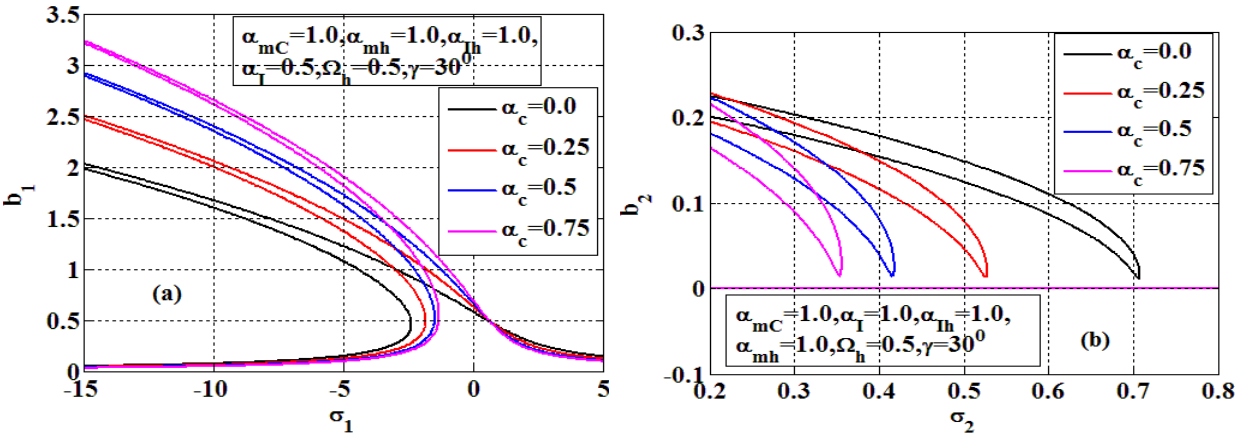

Fig. 3.30: Variation of frequency response curves with offset ratio (α_c) for (a) primary and (b) sub-harmonic resonance.

It is noticeable from Fig. 3.31 that the amplitude increases with the increase in stiffness of hub for the primary resonance case. Hence, with increase in hub-stiffness, frequency Ω_h also increases in a linear proportion. Since with increase hub stiffness, natural frequency is found to be increased and as result, the jump down phenomenon starts at a higher frequency for larger hub stiffness.

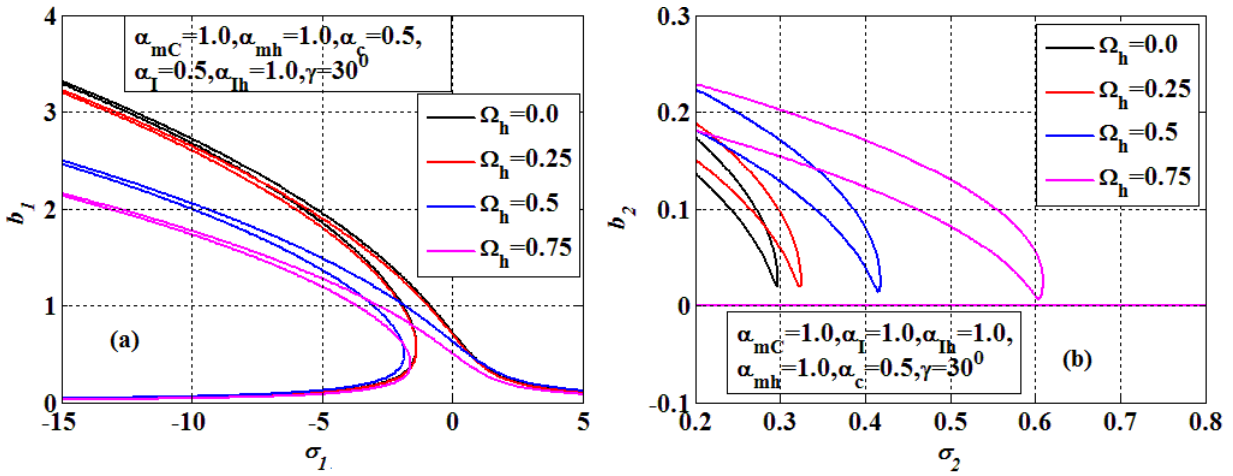

Fig. 3.31 : Variation of frequency response curves with frequency parameter (Ω_h) for (a) primary and (b) sub-harmonic resonance.

3.5 SUMMARY

The present work has shown an extensive effort to highlight the significance of generic payload on the determination of modal characteristics of a flexible manipulator with bi-directional base motion. The evaluation of modal parameters is essential for the behavior estimation of manipulator system when it is externally excited and the frequency of the excitation becomes nearly equal to the system natural frequency. The small deformation model using nonlinear Euler-Bernoulli element has been derived with the account of geometric nonlinearity arising due to mid-plane stretching for rotating Cartesian manipulator with a pulsating constraint force. For manipulator with revolute joint, a large deflection model of a flexible manipulator considering both transverse and axial deformation, dynamics of rotating hub, generic payload, i.e., offset payload, and rigid motion of platform has been derived. The extended Hamilton's principle is used to obtain the governing equations and boundary conditions. Subsequently, the eigenfrequencies and mode shapes have been developed in terms of essential system parameters.

The longitudinal and transverse motion of the manipulator gets coupled for the non axial offset of the payload. The eigenfrequencies of the system tend to decrease as the offset mass, actuator mass, inertia and offset length increase. However, increase in actuator stiffness results in the increase of eigenfrequencies of the single-link manipulator. When the system frequency equals the natural frequency of the hub and actuator spring-inertia system, the manipulator vibrates at one mode higher as compared to the values of frequency parameter less than unity. The variation of the actuator mass affected the amplitude of the roller-supported end with a marginal effect on amplitude of payload end. The amplitude of the mode shapes is significantly affected by the consideration of generic payload as compared to point payload condition. The change in offset parameters has shown a significant effect on modal deflection and angular position of the manipulator affecting the maximum overshoot and settling time when a smooth sinusoidal torque is applied at the hub-end. It has been observed that the system behavior can easily be controlled by adjusting the system parameters such as payload mass, payload inertia actuator inertia and offset ratio.

The bifurcation diagrams provided a useful insight into the nonlinear dynamic behavior under primary, subharmonic and combined resonance conditions due to the externally applied pulsating force and joint motions. Geometric and inertial nonlinearities induce the multiple solutions which further leads to system bi-stability through saddle-node and pitchfork bifurcations resulting in jump phenomena. The response curves have been observed to exhibit an adverse behavior with a variation from spring hardening to spring softening or vice-versa for the Cartesian manipulator with the change in payload mass, actuator mass and offset ratio. The revolute manipulator with large deformation model exhibit only spring softening behavior. Also, with increase in payload mass, hub inertia and axial offset ratio witness an increase in response amplitude and the jump length. The behavior alterations in response with payload parameters and sudden change in amplitude at the saddle-node and pitchfork bifurcation points may lead to a catastrophic failure under periodical operation of the manipulator with the revolute and Cartesian joint motions.